Hindawi
Geofluids
Volume 2023, Article ID 4270521, 21 pages
https://doi.org/10.1155/2023/4270521

Research Article

Geomechanical Characteristics and Stimulation of Dibei Deep Tight Sandstone Reservoirs in the Kuqa Depression of Tarim Basin

Ke Xu, Haijun Yang, Hui Zhang, Zhimin Wang, Lu Fang, Guoqing Yin, and Haiying Wang

Research Institute of Exploration and Development, Tarim Oilfield Company, PetroChina, Korla, Xinjiang 841000, China

Correspondence should be addressed to Ke Xu; xukee0505@163.com

Received 26 August 2022; Accepted 13 October 2022; Published 20 February 2023

Academic Editor: Peng Tan

Facing the problem of increased production of deep tight gas reservoirs, this study takes the Dibei gas reservoir in Tarim Basin as an example, carries out geomechanical research, and reveals the rock mechanical properties, in situ stress, and fracture characteristics of the tight reservoir. From the perspective of the in situ stress field and the effectiveness of fractures, the study reveals their impacts on reservoir quality, wellbore stability, and fracturing networks. The results show that the in situ stress and the effectiveness of fracture mechanics under its control have obvious control over the production capacity in the Dibei gas reservoir. The positions and intervals with low in situ stress, high fracture density, and fracture effectiveness are often favorable parts. A directional well has the dual advantages of overcoming reservoir heterogeneity and safety and stability. Understanding the geomechanical characteristics can quantitatively optimize the best wellbore trajectory, reduce the difficulty of fracturing from the source of well location deployment, improve the efficiency of hydraulic fracturing, and then realize the stimulation of gas reservoirs. In addition, the favorable borehole trajectory considers both the sweet spot penetration and borehole wall stability, which will reduce the difficulty of fracturing and is conducive to the efficient stimulation of tight gas reservoirs. Geomechanics research has built an integrated bridge between geology and engineering, which plays a significant role in increasing gas production.

1. Introduction

In recent decades, unconventional resources have attracted extensive attention. Global oil and gas exploration and development are continuously extending from conventional to unconventional counterparts [1–3]. The role of unconventional oil and gas production is continuously strengthened, with resources accounting for approximately 80% of the total oil and gas resources [3, 4].

Unconventional resources mainly include tight oil and gas, shale oil and gas, and coalbed methane, and most of these reservoirs are extremely tight. Generally, the permeability of tight sandstone and tight carbonate matrix is less than $0.1 \times 10^{-3}\ \mu m^2$, and the permeability of shale matrix is even less than $0.001 \times 10^{-3}\ \mu m^2$. There is no natural production capacity in a single well, and it is difficult to obtain natural industrial production by traditional technology [3]. New technology is required to improve reservoir permeability or fluid viscosity to realize economic exploration. Typically, these measures include acid fracturing, multistage fracturing, horizontal boreholes, multibranch boreholes, and "artificial permeability" through horizontal borehole platform volume fracturing.

In the early stage of exploration and development of unconventional resources, the understanding of reservoir geology was insufficient, and engineering technology was limited, which hindered the economic oil and gas production of these resources. In recent years, with the progress of science and technology, scholars have gradually realized that mechanical issues always exist during the whole

exploration and exploitation of unconventional resources, involving structural geology, petroleum geology, rock mechanics, and petroleum engineering [5–8]. Geomechanics is of great significance to guide unconventional oil and gas exploration and development through studies on reservoir rock mechanical property analysis, in situ stress field simulation, fault sealing evaluation, fracture activity prediction, borehole stability analysis, hydraulic fracture propagation, casing damage prediction, and protection [9–16].

China is rich in unconventional oil and gas reservoir resources, with onshore shale oil resources up to 283×108 t [4]. The Tarim Basin in western China is the largest petroliferous basin in China. The Kuqa Depression in the northern Tarim Basin is rich in tight oil and gas and coalbed methane resources. However, due to the large burial depth of the gas reservoir, complex geological background, extremely strong structural compression, well-developed faults, and fractures, understanding of the controlling factors for the gas reservoir and the distribution of oil and gas is unclear.

Therefore, taking the Dibei tight sandstone gas reservoir as an example, based on the analysis of reservoir characteristics, this paper carries out geomechanical research; reveals the rock mechanical properties, in situ stress, fracture development, and effectiveness of tight reservoirs; and proposes a technique to increase the production of tight reservoirs considering geomechanical factors. This study reveals the impact of the in situ stress field and fracture activity on reservoir quality, borehole wall stability, and fracturing network; quantitatively optimizes the best borehole trajectory; considers favorable reservoir penetration; reduces complex drilling accidents; and improves the fracturing effect to realize the stimulation of deep tight sandstone gas reservoirs.

2. Geological Setting

2.1. Location and Structural Features. Tarim Basin is located in northwest China and can be divided into seven first-order structural units (Figure 1(a)). The Kuqa Depression is on the northern edge of the Tarim Basin, which is divided into seven second-order structural units and shows the structural pattern of "four belts and three depressions" [17] (Figure 1(b)). The northern monoclinal belt is located at the northernmost end of the Kuqa Depression. It is 420 km long in the east–west direction and 5~20 km wide in the north-south direction, covering an exploration area of 8200 km^2 [18]. It is divided into three tectonic sections from west to east: the Bashi section, Dibei section, and Tuzi section [18–20] (Figure 1(c)).

The northern monoclinal belt, close to the South Tianshan orogenic belt, has experienced multistage tectonic movement with complex tectonic deformation. The Dibei block is ~E–W-trending and is generally characterized by a south-dipping monocline, in which many ~E–W faults are developed. According to the development characteristics of faults and their relationship with oil and gas, the faults in the Dibei gas reservoir are generally divided into three levels (Figure 2): Level I—fault controls the structural boundaries and destroys the oil and gas reservoir; Level II—fault controls the distribution of the belt to communicate oil and gas sources; and Level III—fault controls oil and gas enrichment [18].

2.2. Strata. The strata in the Dibei block include (Figure 3) Quaternary Xiyu Formation (Q_1x), Neogene Kuqa Formation (N_2k), Kangcun Formation ($N_{1\text{-}2}k$), Jidike Formation (N_1j), Paleogene Suweiyi Formation ($E_{2\text{-}3}s$), Kumugeliemu Group ($E_{1\text{-}2}km$), Cretaceous Shushanhe Formation (K_1sh), Yageliemu Formation (K_1y), Jurassic Qigu Formation (J_3q), Chakemake Formation (J_2q), Kezilenuer Formation (J_2kz), Yangxia Formation (J_1y), Ahe Formation (J_1a), Triassic Taliqike Formation (T_3t), Huangshanjie Formation (T_3h), Kelamayi Formation (T_2kl), and Ehuobulake Formation (T_1eh). The main oil- and gas-bearing layers include J_1a, J1y, and J_2kz, and the local areas include N_1j. Oil and gas are mainly from lacustrine mudstone of the Upper Triassic and coal measured strata of the Middle and Lower Jurassic, with great thickness and high abundance of organic matter. Multiple sets of source rocks and Middle-Lower Jurassic reservoirs are superimposed in a "sandwich" manner, forming two sets of high-quality source reservoir cap assemblages: the first set takes the T_3h and T_3t as the source layers, the J_1a sandy conglomerate as the reservoir and the J_1y coal measure stratum as the cap rock; the second set takes the coal measure strata of J_1y and J_2kz as the source layers, sandstones of J_1y and J_2kz as the reservoir, and the mudstone of Jurassic J_2q and J_3q as the caprock [20].

2.3. Reservoir Characteristics. The main exploration layer in the Dibei gas reservoir is J_1a, which is dominated by braided river delta plain subfacies (Figure 4), and the sand bodies are staggered and overlap vertically and horizontally, with a thickness of 260~300 m [18]. It is mainly composed of gravel, gravelly coarse sandstone, and coarse sandstone. Overall, J_1a is characterized by multicycle superposition. For the single cycle, a small extension distance, rapidly changing lithology and grain size, and frequent spatial migration lead to strong reservoir heterogeneity (Figure 5).

The rock-type J_1a in the Dibei gas reservoir is mainly lithic sandstone. The reservoir space is mainly intragranular dissolved pores and micropores, accounting for 37.36% and 34.23%, respectively, followed by intergranular dissolved enlarged pores, accounting for 20.09%. Microfractures are relatively developed and can communicate with pores. The effective reservoir porosity of J_1a ranges between 4.0% and 13.9%, with an average of 6.6% and a median of 6.4%. The permeability ranges between 0.170×10^{-3} μm^2 and 9.898×10^{-3} μm^2, with an average of 1.577×10^{-3} μm^2 and a median of 0.934×10^{-3} μm^2. It generally belongs to ultralow porosity, low-ultralow permeability sandstone reservoirs, and tight sandstone reservoirs.

3. Geomechanical Analysis Method

3.1. Rock Mechanical Parameters. The commonly used rock mechanical parameters are generally Young's modulus of

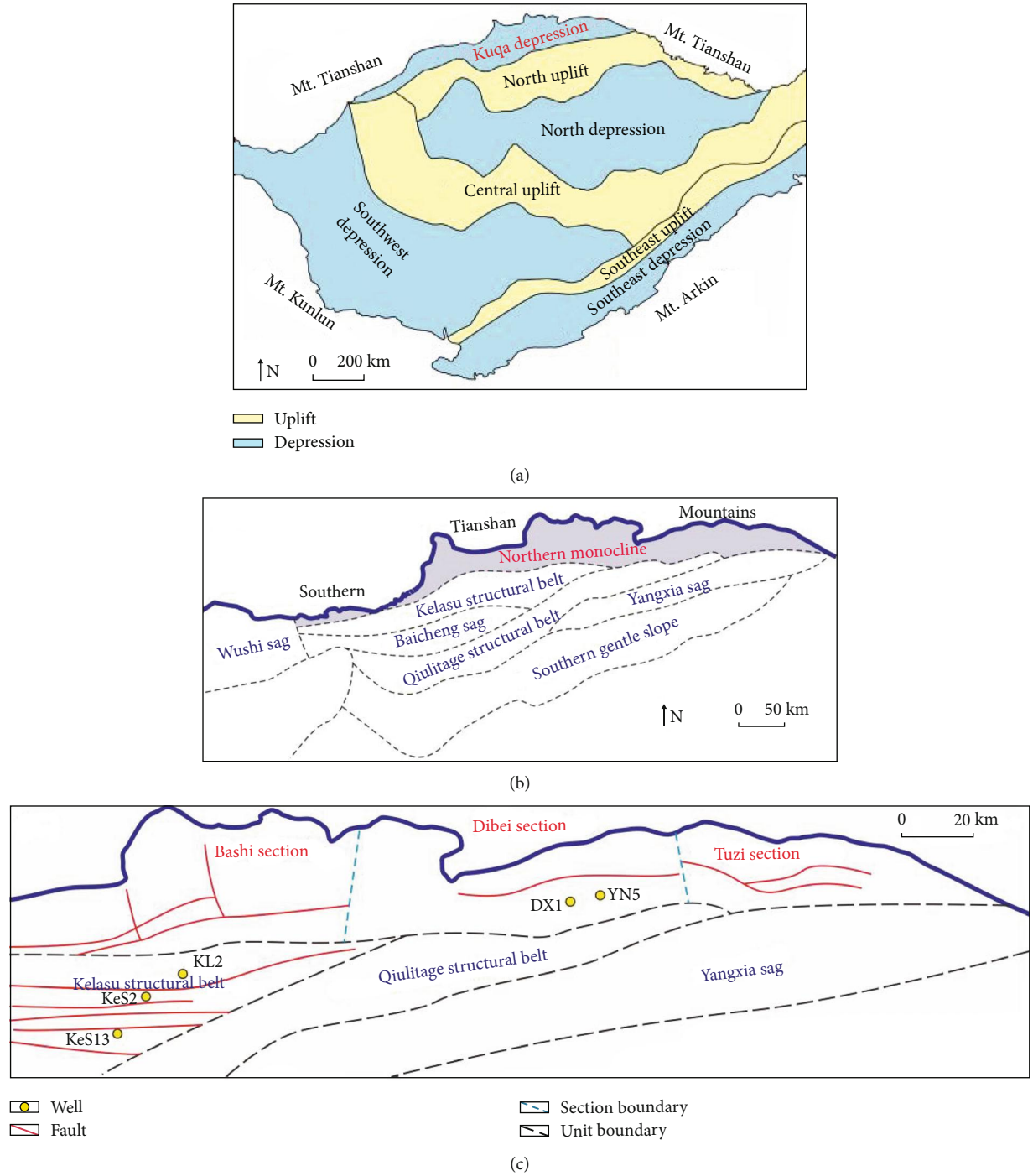

Figure 1: Division of structural units in the Kuqa Depression and structural location of the Dibei gas reservoir. (a) The Kuqa Depression is located in the northern margin of Tarim Basin, and it is divided into seven first-order structural units, which are the Kuqa Depression, Northern Uplift, Northern Depression, Central Uplift, Southwestern Depression, Southeastern Uplift, and Southeastern Depression; (b) the Kuqa Depression is divided into seven second-order structural units, which are the northern monoclinal belt, Kelasu tectonic belt, Qiulitage tectonic belt and southern slope belt, the Wushi sag, Baicheng sag, and Yangxia sag; (c) the northern monoclinal belt is divided into three tectonic segments: the Bashi section, Dibei section, and Tuzi section.

elasticity, Poisson's ratio, density, internal friction angle, cohesion, and compressive strength. Reservoir rock mechanical parameters are closely related to in situ stress and fractures. They are the main basis for numerical simulation of basin tectonic stress fields and reservoir fractures, drilling design of oil and gas wells, and reservoir hydraulic fracturing design.

Rock mechanical parameters can be calculated with two methods. The first method is to carry out rock mechanical tests of rock samples in the laboratory, including uniaxial

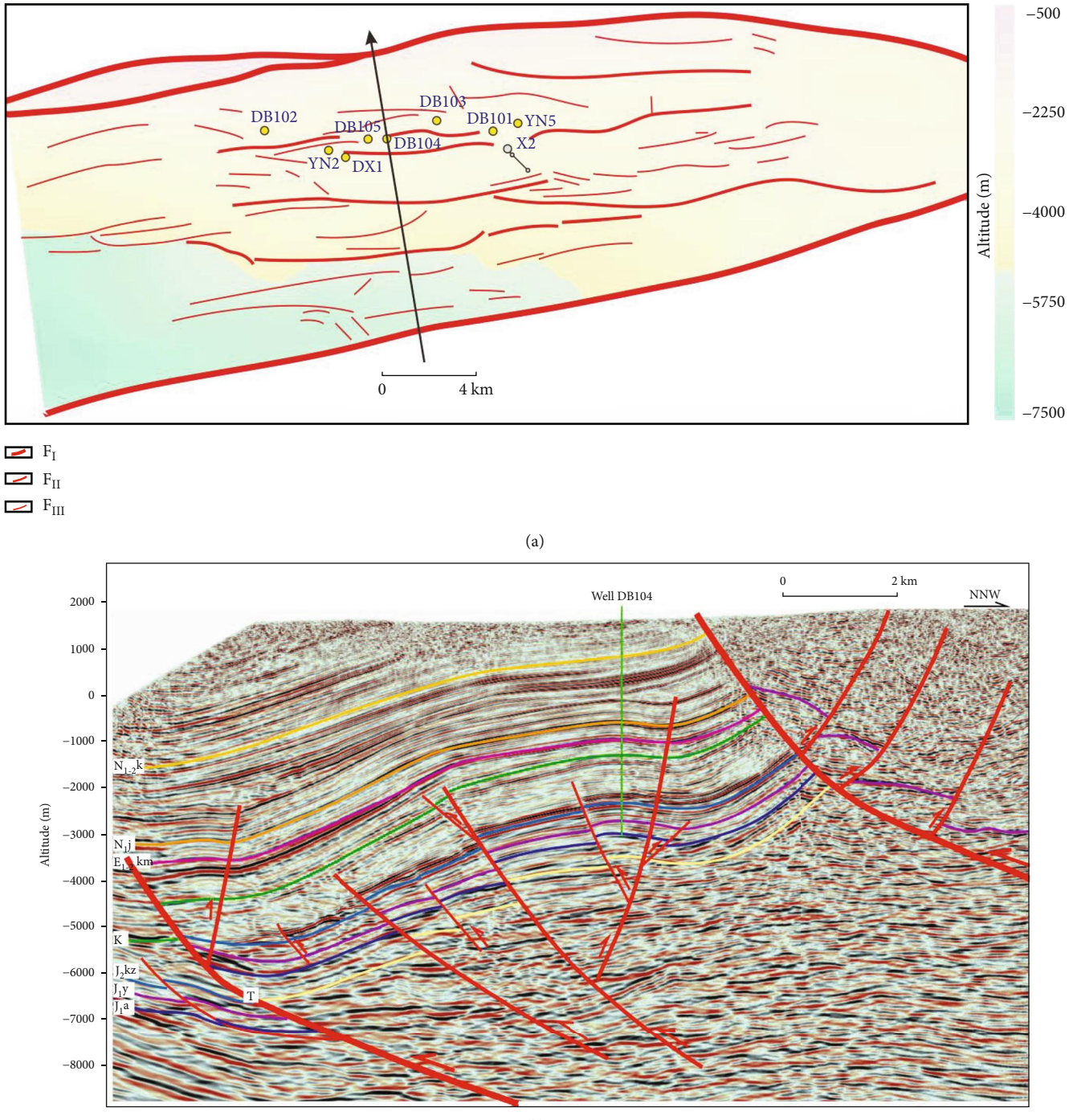

Figure 2: Top structural map and seismic profile of the Jurassic Ahe Formation in the Dibei gas reservoir. (a) There are many faults in the Dibei gas reservoir, which are generally divided into three levels. (b) The Dibei block is characterized by a south-dipping monocline.

compression tests and triaxial compression tests. The second is to calculate by using geophysical data and the corresponding calculation model. For deep reservoirs, drilling and logging data are generally used to calculate rock mechanical parameters because deep gas reservoirs are characterized by high stress and difficulty in removing cores. Even if the cores can be removed, the rapidly released stress results in inaccurate measurements or possible core fracture. Drilling and logging data make up for the deficiency of rock mechanics to a certain extent, offering the advantages of good continuity and low cost.

In this paper, XMAC logging is used to analyze the mechanical properties of rocks, and unipolar acoustic transmitter is used in ordinary acoustic logging, which can emit

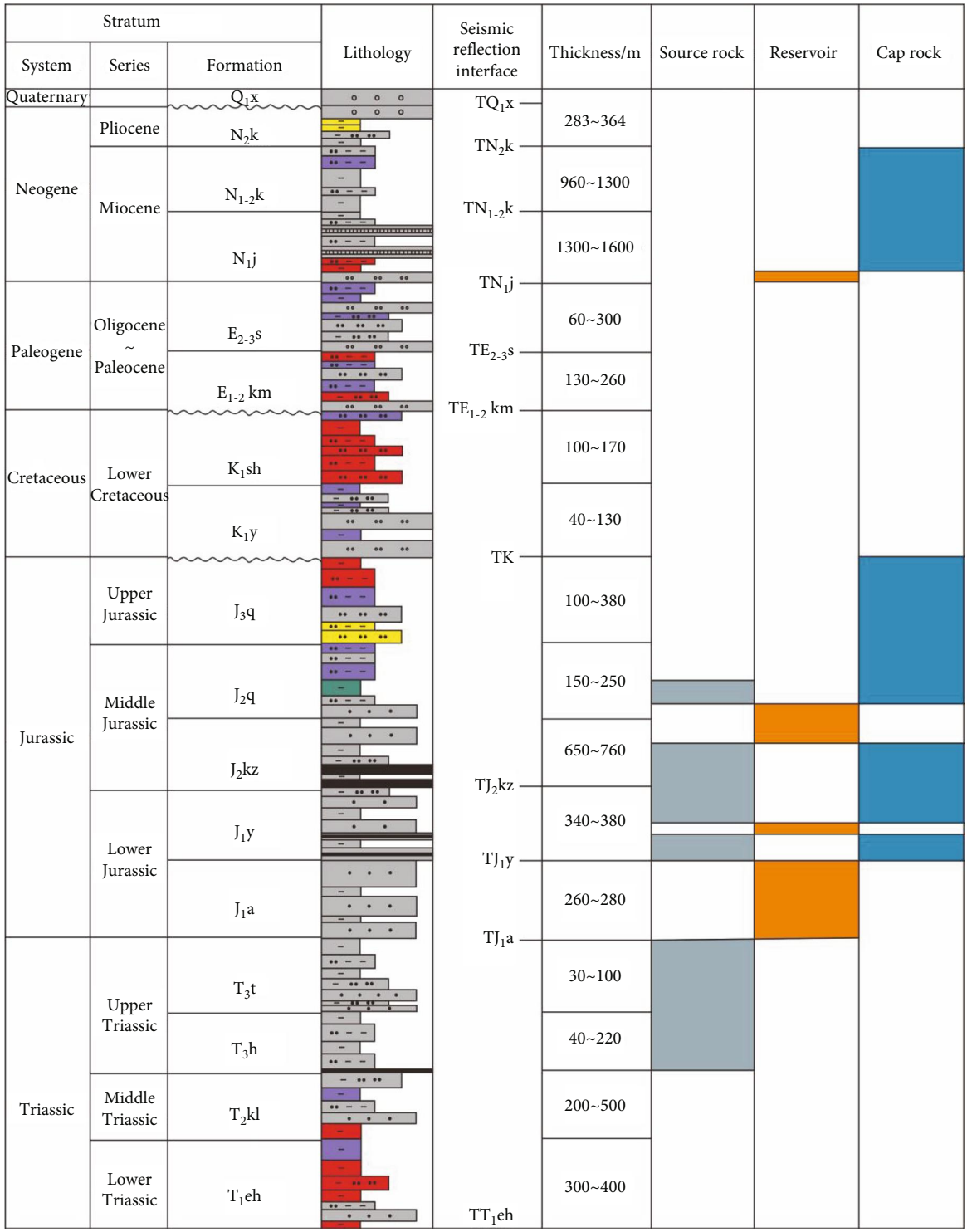

Figure 3: Mesozoic Cenozoic stratigraphic system in the northern tectonic belt of the Kuqa Depression [20].

acoustic waves to the borehole wall, causing slight wellbore expansion. Therefore, P-wave and S wave reach the stratum and obtain the time difference between P-wave and S-wave. Cross-multipole array acoustic logging is the best method to measure formation P wave, S wave, and Stoneley wave and can provide data describing formation anisotropy.

XMAC logging mainly uses full acoustic data to extract P-wave slowness, S-wave slowness, and Stoneley wave slowness. Rock mechanics parameters are calculated based on the extracted P-wave slowness, S-wave slowness data, and available rock density. All wells in this paper have XMAC logging, which is conducive to the calculation of rock

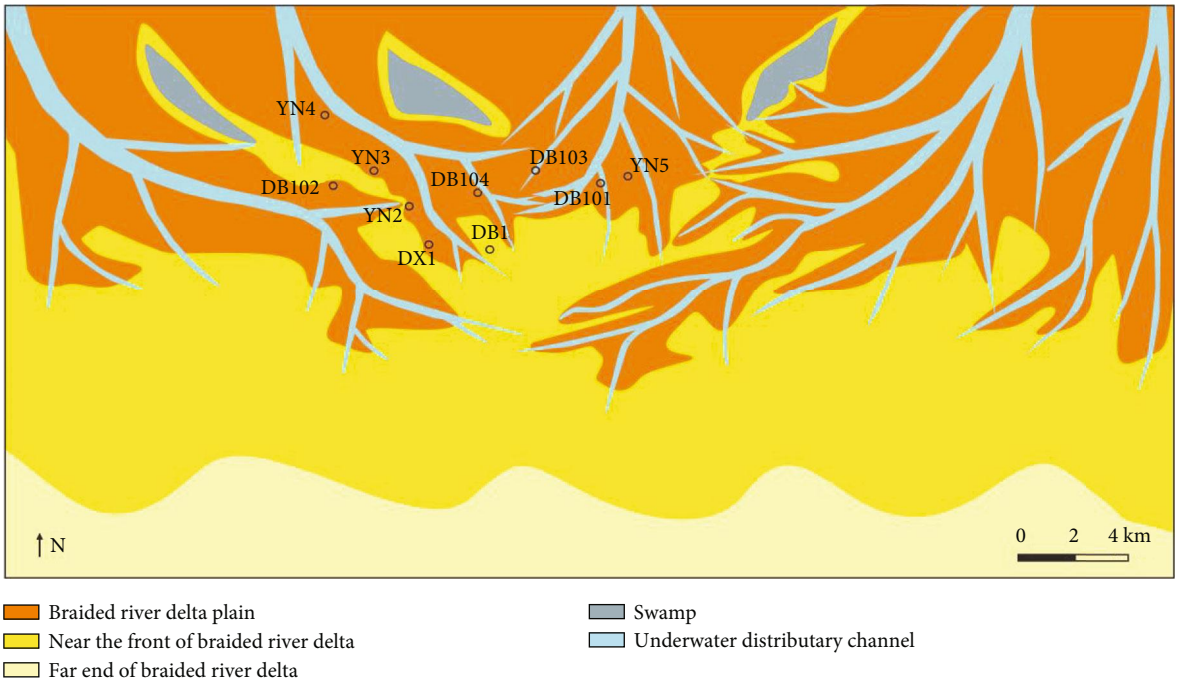

Figure 4: Distribution of Jurassic sedimentary facies in the Dibei block.

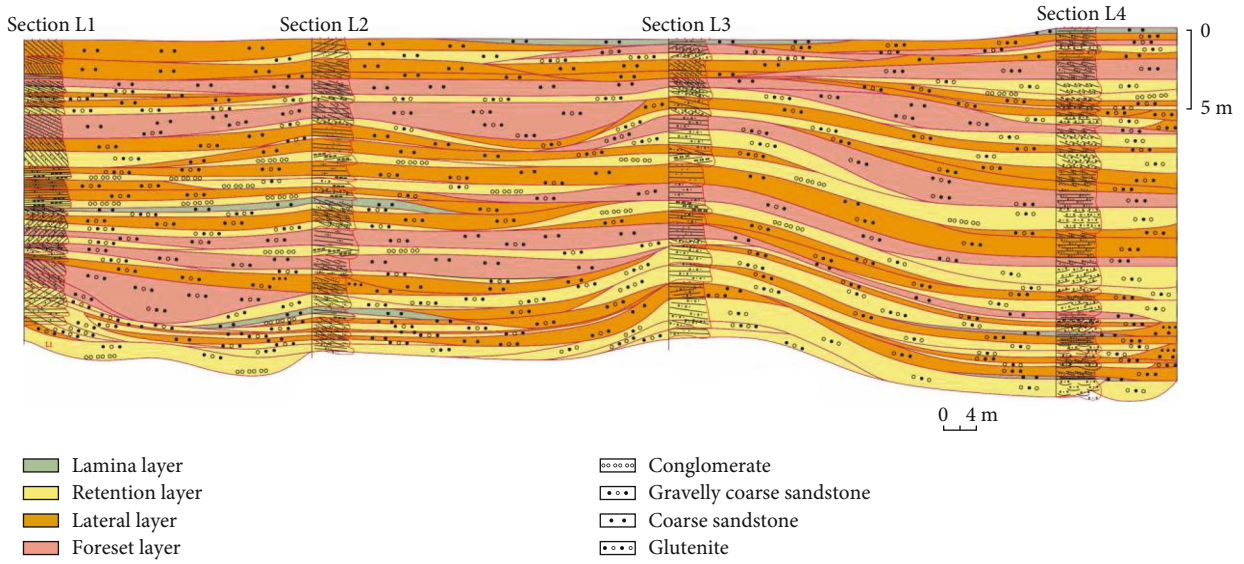

Figure 5: Outcrop characteristics of the Jurassic Ahe Formation in the Kezilenuergou area [18].

mechanical parameters. The elastic modulus (E) and Poisson's ratio (μ) are calculated as follows [21–23]:

$$E = \frac{\rho_b}{\Delta t_s^2} \cdot \frac{3\Delta t_s^2 - 4\Delta t_p^2}{\Delta t_s^2 - \Delta t_p^2},$$
$$\mu = \frac{\Delta t_s^2 - 2\Delta t_p^2}{2\left(\Delta t_s^2 - \Delta t_p^2\right)}, \quad (1)$$

where ρ_b is rock density (kg/m^3) and Δt_p and Δt_s are P-wave time difference and S-wave time difference, respectively (μs/ft).

The calculation formula of uniaxial compressive strength (UCS) applicable to Cretaceous strata in the Kuqa Depression is

$$\mathrm{UCS} = 7 \times 10^{-6} \times \left(0.00175 \times \rho_b \times {V_p}^2 \times 0.145 - 3043\right) - 20.961. \quad (2)$$

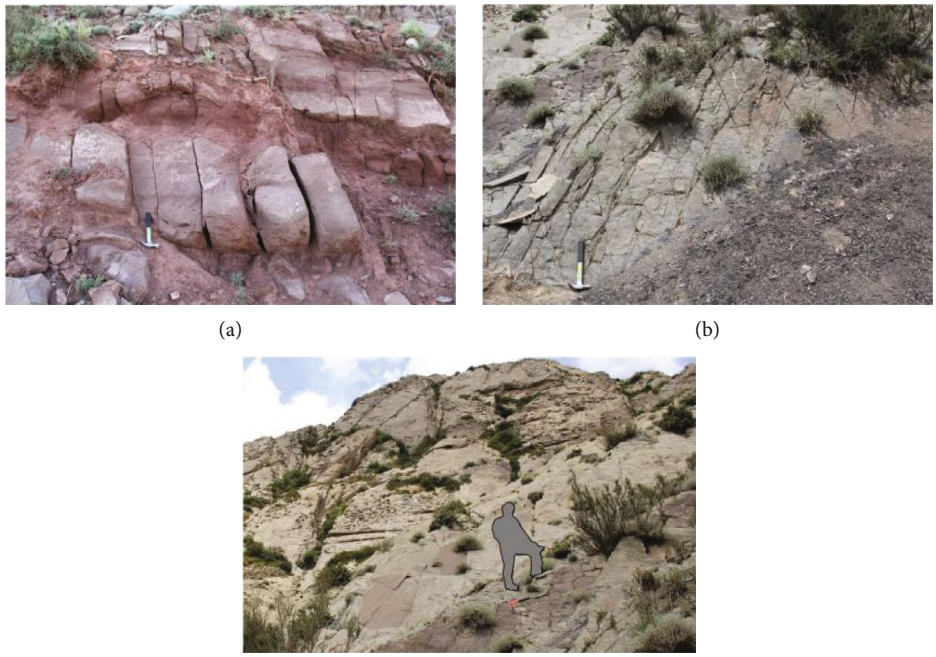

(a) (b)

(c)

Figure 6: Typical outcropping fractures in the Dibei area. (a) Fractures are only developed in sandstone; they stop at the interface between sandstone and mudstone in the Kalazha Formation of the Jurassic. (b) Typical conjugate shear fractures in the Ahe Formation of the Jurassic. (c) Large-scale shear fractures extending tens of meters in the Ahe Formation of the Jurassic.

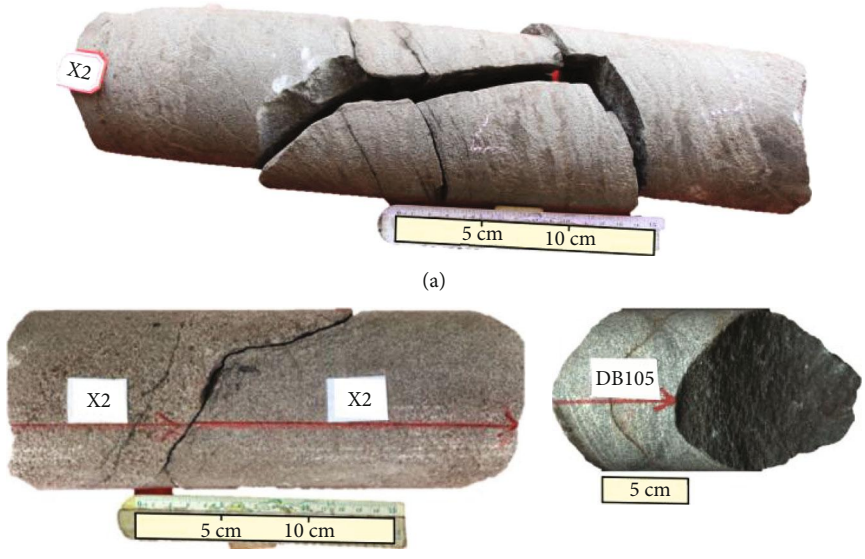

(a)

(b) (c)

Figure 7: Typical fractures in drilling cores. (a) Well X2, 5110.2~5110.6 m; the formation of Jurassic; it can be seen as high angle shear fracture and a group of low angle interlayer fractures; the interlayer fractures are filled with argillaceous and carbonaceous materials. (b) Well X2, 5122.2~5122.4 m; Ahe formation of Jurassic, a curved shear fracture with medium-high angle, unfilled. (c) Well DB105, 4759 m~4767.5 m, Ahe formation of Jurassic, a group of parallel low angle fractures is developed, the coal is fully filled, and the core is fractured along the fracture.

3.2. In Situ Stress. In general, the in situ stress tensor is used to describe the in situ stress state, which includes the minimum horizontal stress (S_h), maximum horizontal stress (S_H), and vertical stress (S_v) [24].

The S_v is equal to the gravity of the overlying rock mass, which can be calculated by integrating the density curve from the ground to the target depth such as Equation (3) [15, 25–27]:

$$S_V = \int_0^z \rho(z) g dz, \tag{3}$$

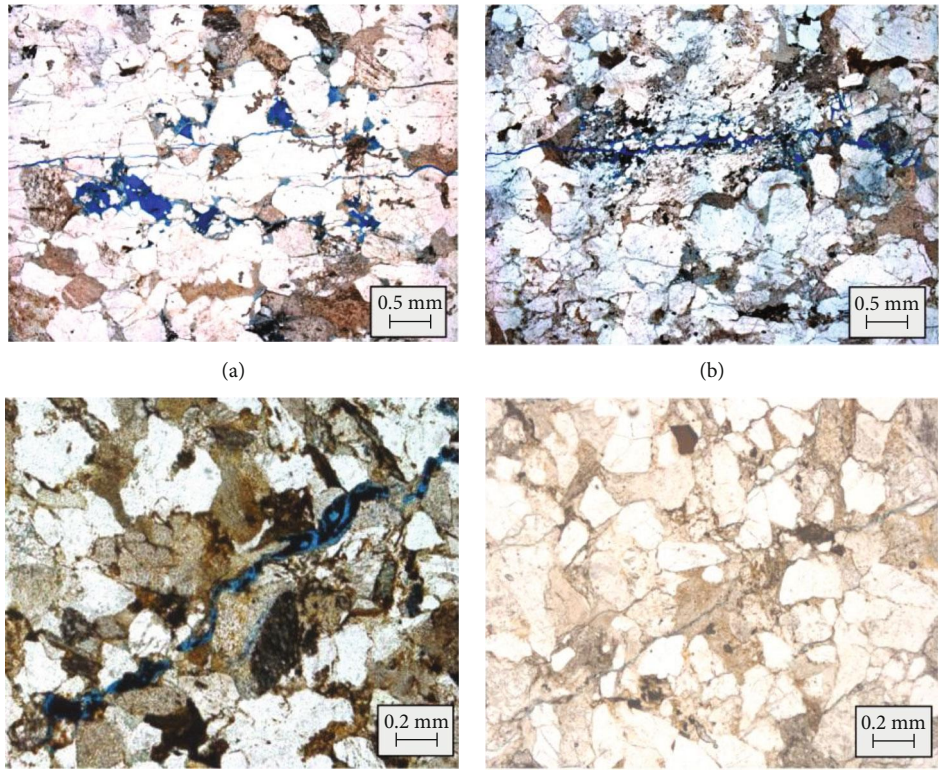

Figure 8: Typical fractures in thin section. (a) Well DB105, 4764.18 m; the formation of Jurassic, coarse-grained lithic sandstone; unfilled microfractures are distributed in parallel layers, and intergranular pores and intragranular dissolved pores are connected with the fractures. (b) Well DB105, 4770.19 m; Ahe formation of Jurassic, under compaction and stress; the particles are in point line contact, and intragranular solution pores and microcracks are developed. The microcracks cut the particles intermittently and extend parallel to the plane with directionality. (c) Well X2, 5129.7 m; the formation of Jurassic Medium sandstone, dense rock, poor pore performance; see a microfracture half filled with asphaltene; (d) YN5, 4561.7 m; Yangxia formation of Jurassic, medium grained sandy structure, dense rock, poor pore performance, and developed microfractures.

where g is the gravitational acceleration (m/s^2), $\rho(z)$ is the density of the overburden rock as a function of burial depth (kg/m^3), and z is the burial depth from the surface to a particular depth underground (m).

For the wells we investigated, density logs were not acquired from the ground level. Ideally, the shallow S_v could be calculated based on a relationship between density and sonic velocity data [26]. However, no velocity data were present between ground level and the first density data point. Hence, an extrapolation method was used in the present study, and a gradient of approximately 23000 Pa/m was identified in the open hole section to determine the S_v.

There are many calculation models for obtaining horizontal principal stress magnitudes, including uniaxial strain model, Mohr Coulomb failure model, Coulomb Navier failure model, Huang's model, combined spring model, porous elastic strain model, and biaxial strain model [28, 29].

According to the production practice experience of Tarim Oilfield Company, the combined spring model assumes that there is no relative displacement between strata in the process of structural movement and considers the influence of elastic modulus on the in situ stress, which is greatly suitable for the Kuqa foreland thrust belt with strong compressions. Therefore, the combined spring model is used to calculate the in situ stress in this paper, and the calculation formula is as follows [28]:

$$\begin{cases} S_H = \dfrac{\mu}{1-\mu}\left(S_V - \alpha P_p\right) + \dfrac{E\xi_H}{1-\mu^2} + \dfrac{\mu E\xi_h}{1-\mu^2} + \alpha P_p, \\ S_h = \dfrac{\mu}{1-\mu}\left(S_V - \alpha P_p\right) + \dfrac{E\xi_h}{1-\mu^2} + \dfrac{\mu E\xi_H}{1-\mu^2} + \alpha P_p, \end{cases} \tag{4}$$

where S_H is the maximum horizontal principal stress (MPa), S_h is the minimum horizontal principal stress (MPa), S_V is the vertical principal stress (MPa), P_P is the pore pressure (MPa), μ is Poisson's ratio (dimensionless), E is the modulus of elasticity (GPa), α is the Biot coefficient (dimensionless), and ξ_H and ξ_h are the maximum and minimum principal stress coefficient, respectively (dimensionless).

Generally, we may determine S_h at a specific location through hydraulic fracturing construction data, which can be used as the constraint and scale basis to determine the value of ξ_h. However, the maximum horizontal principal stress (S_H) of ultradeep wells cannot be determined through hydraulic fracturing [30], because the maximum horizontal

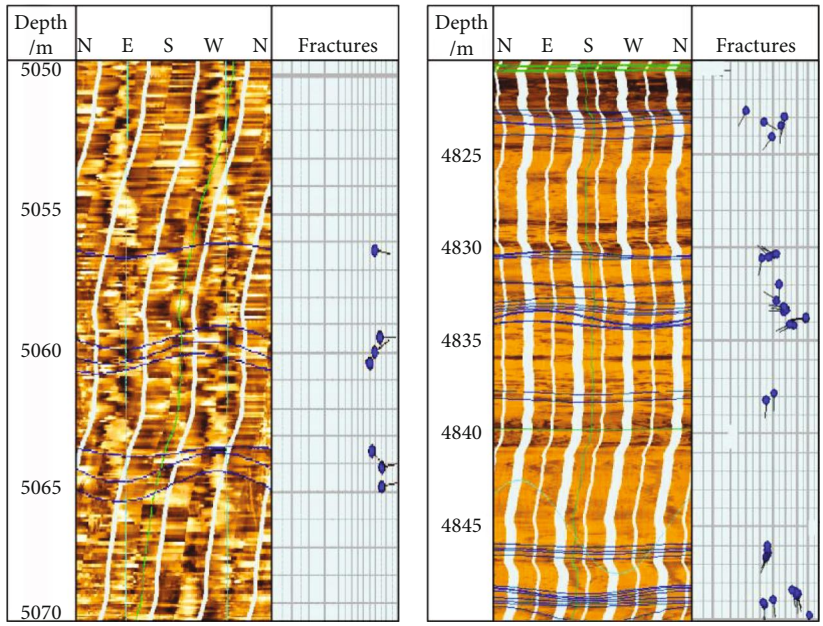

Figure 9: Fracture identification with imaging logging. (a) Well BD102, 5055-5070 m; Ahe Formation of Jurassic. (b) Well DX1, 4820-4850 m; Ahe Formation of Jurassic.

principal stress only can be accurately measured according fracturing curve with small displacement. Therefore, the S_H is determined with wellbore fracture information in this paper. The stress distribution around the wellbore is no longer uniform under the in situ stress. Affected by the orientation of the in situ stress and the distance from the borehole wall, stress concentration and tension occur in the S_h and S_H directions, respectively. When the stress concentration exceeds the strength of the rock around the borehole, borehole wall collapse occurs. The stress distribution around the borehole varies in different lithologic sections at different structural parts, and the borehole wall collapse may also show differences [10]. The collapse width of the borehole wall can be judged from imaging logging data, and there is a quantitative mathematical calculation relationship between collapse width, uniaxial compressive strength, and in situ stress state [30]. Therefore, the magnitude and orientation of in situ stress can be reverted by the collapse width and the uniaxial compressive strength of the borehole collapse position.

3.3. Fracture Identification and Effectiveness Evaluation. Fracture identification methods generally include (1) identifying macro large-scale fractures through outcrops, studying the occurrence and scale of fractures, genetic types and formation environment of fractures, distribution characteristics, and mutual relationship of fractures in different formations, formation stages of fractures, and the relationship between different parameters of fractures (Figure 6); (2) observing fractures in drilling cores which is the most visual method to identify reservoir fractures (the mechanical type, occurrence, opening length, density, filling characteristics, and other parameters can be obtained (Figure 7)); (3) thin section observation of microfractures, including intragranular fractures and grain edge fractures (Figure 8); and (4) logging data interpretation and imaging logging which is generally used to identify fractures. Its principle is based on the resistivity difference between the surrounding rock and fracture. It is easier to identify the fracture if the difference between borehole wall rock resistivity and drilling fluid resistivity is greater (Figure 9).

Fracture effectiveness determines the flow capacity of deep fractured reservoirs and affects oil and gas productivity [31–36]. Factors affecting fracture effectiveness include fracture density, opening, filling, and fracture shear slip ability under an in situ stress environment, that is, mechanical effectiveness [37–39]. Since the Kuqa Depression experiences extremely strong tectonic compression, the in situ stress environmental factors of deep reservoirs are fully considered. In this paper, the shear-slip of fractures under the control of in situ stress is analyzed from the perspective of geomechanics, the fracture opening pressure is simulated, and the effectiveness of reservoir fractures is comprehensively evaluated.

The stress tensor on the fracture surface may be decomposed into normal stress (σ_n) and shear stress (τ) under the control of in situ stress; σ_n is perpendicular to the fracture surface, and τ is parallel to the fracture surface. The shear slip ability of fractures can be affected by the ratio of shear stress to effective normal stress (τ/σ_{ne}), which reflects the permeability of the fracture to some extent [40], and generally, a higher ratio indicates a better fracture effectiveness.

In addition, based on the critical stress fracture hypothesis [41, 42], it is considered that the fracture that reaches the critical stress will have a certain permeability. Whether

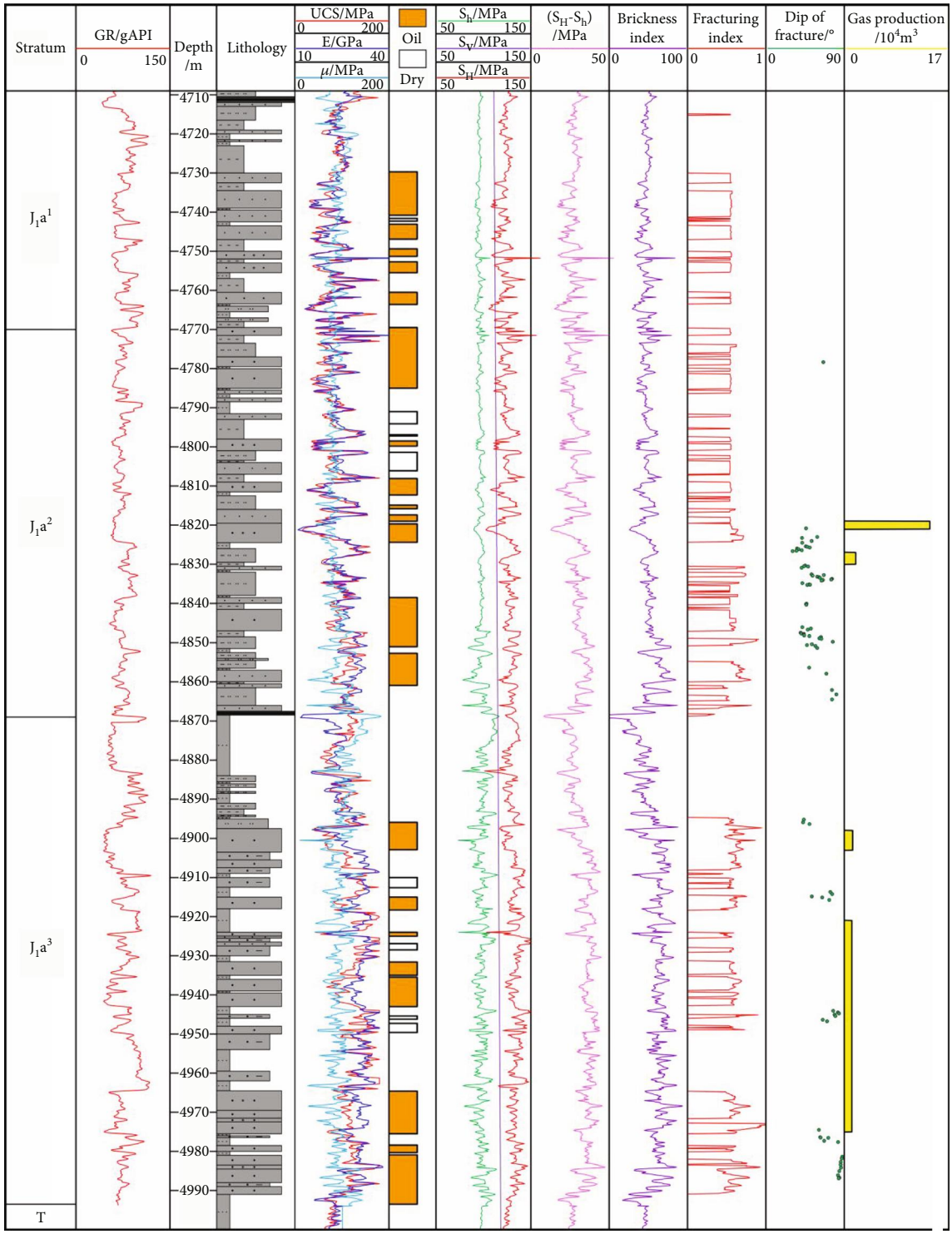

Figure 10: Geomechanical histogram of Well DX1.

it reaches the critical stress is determined by the ratio of the shear stress to the effective normal stress. Based on the research of Byerlee et al. [43] and Zoback [30], it is considered that fractures with a friction coefficient of fracture surface less than 0.6 do not have permeability and only those fractures with a friction coefficient greater than 0.6 and less than 1 have a certain permeability. With the development of exploration, the fracture shear slip ability can be enhanced by increasing the pore pressure through hydraulic fracturing, and the fracture permeability may clearly improve.

3.4. Fracturing Ability. The natural productivity of the Dibei tight gas reservoir is extremely low, and fracturing is required to obtain productivity. Fracturing ability is a

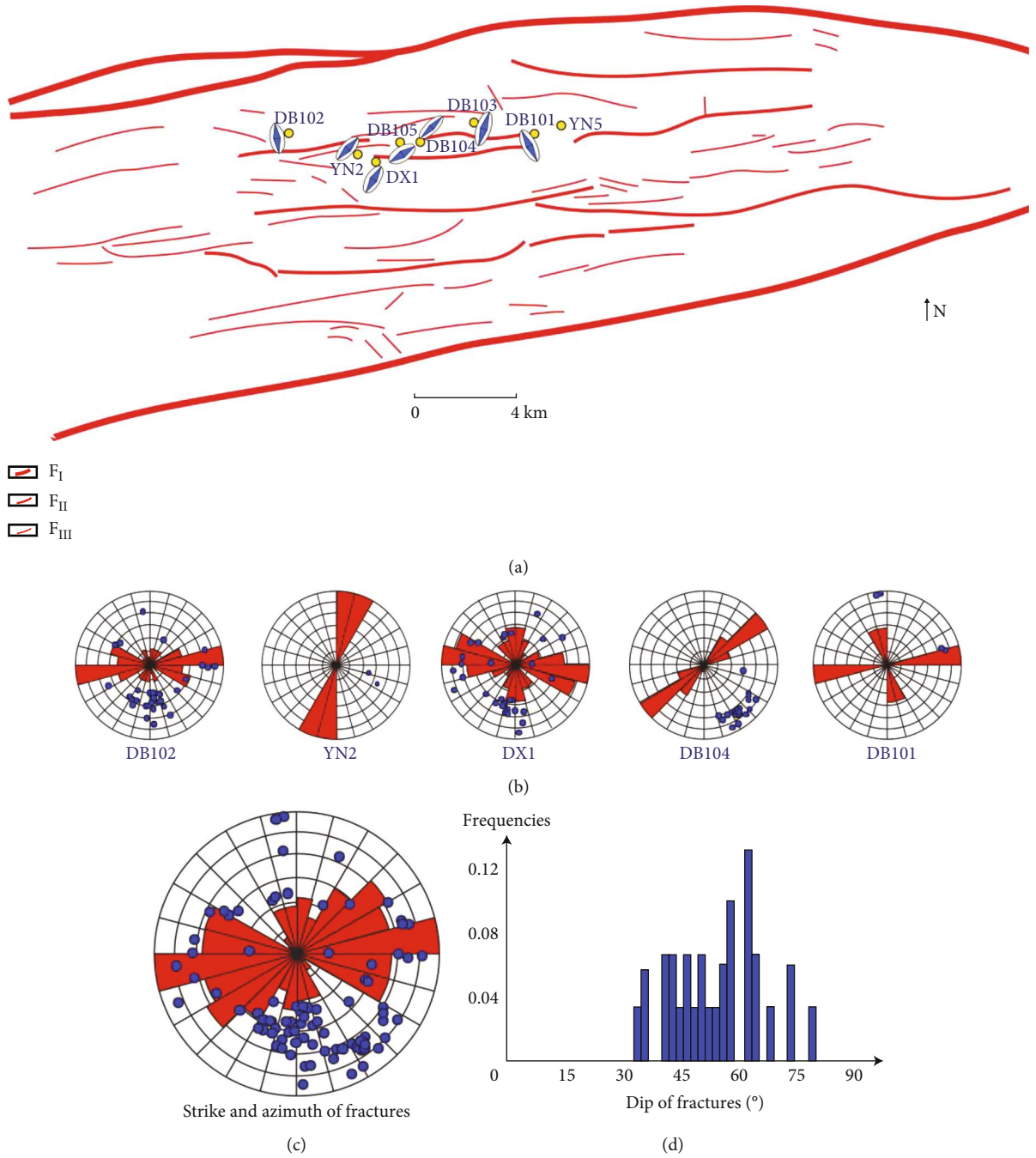

Figure 11: Orientation of S_H and fracture strike of the Dibei gas reservoir.

parameter used to evaluate whether a reservoir can be effectively fractured in hydraulic fracturing. It is a basis for the design and optimization of reservoir transformation schemes, and the brittleness of rock is first considered the key parameter to characterize the difficulty of fracturing in shale gas development [44–47]. Rock mineral composition and rock mechanical parameters are mainly used to evaluate the brittleness of shale [48, 49]. However, under some special conditions, rock brittleness cannot truly reflect the fracturing ability of the formation. For example, a dolomitic limestone layer of the Carboniferous Barnett Formation in the Fort Worth Basin of the United States has high brittleness, but in actual fracturing, the layer is a barrier to fracturing. Under the same injection pressure, it is more difficult to breakdown shale formations than shale formations with low brittleness [48, 50]. In addition, this situation also occurs in Well Luntan 1, an ultradeep well located in the Tarim Basin of China. The dolomite with high brittleness cannot be broken down. Zhang et al. [50] believed that, in addition to rock brittleness, fracture toughness, in situ stress, and the effectiveness of fracture mechanics also affect the fracturing ability of deep tight reservoirs with high-stress and well-

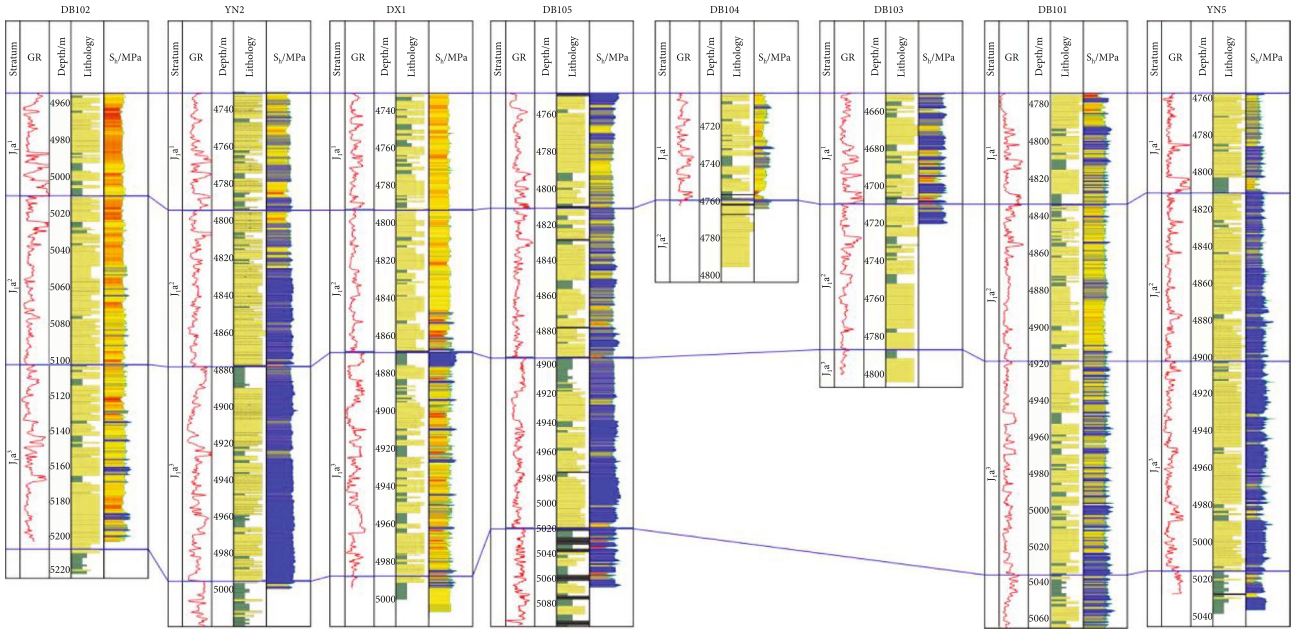

Figure 12: In situ stress profile of typical wells in the Dibei gas reservoir.

developed fractures. Therefore, the calculation method of the fracturing capability index (I_{Frac}) is proposed:

$$I_{\text{Frac}} = W_1 \frac{(S_h)_{\max} - S_h}{(S_h)_{\max} - (S_h)_{\min}} + W_2 \frac{(\tau/\sigma_{ne}) - (\tau/\sigma_{ne})_{\min}}{(\tau/\sigma_{ne})_{\max} - (\tau/\sigma_{ne})_{\min}} + W_3 \frac{I_B - (I_B)_{\min}}{(I_B)_{\max} - (I_B)_{\min}} + W_4 \frac{(K_{IC})_{\max} - K_{IC}}{(K_{IC})_{\max} - (K_{IC})_{\min}}, \tag{5}$$

where $(S_h)_{\max}$ and $(S_h)_{\min}$ are the maximum and minimum of S_h, respectively; $(\tau/\sigma_{ne})_{\max}$ and $(\tau/\sigma_{ne})_{\min}$ are the maximum and minimum of τ/σ_{ne}, respectively; $(I_B)_{\max}$ and $(I_B)_{\min}$ are the maximum and minimum values of I_B, respectively; $(K_{IC})_{\max}$ and $(K_{IC})_{\min}$ are the maximum and minimum values of K_{IC}, respectively; and W_1, W_2, W_3, and W_4 are the weight coefficients of four factors, respectively, which are generally taken as 0.25. At the same time, with reference to the stress state of a single well, fracture development, and rock mechanical attribute characteristics, the weight of a parameter may be increased or reduced according to experience, and it shall meet $W_1 + W_2 + W_3 + W_4 = 1$.

The brittleness index (I_B) in Equation (5) is calculated as follows:

$$I_B = A_1 \times \frac{E - E_{\min}}{E_{\max} - E_{\min}} + A_2 \times \frac{\mu_{\max} - \mu}{\mu_{\max} - \mu_{\min}}, \tag{6}$$

where $E_{\max}$ and $E_{\min}$ are the maximum and minimum of the elastic modulus of the calculated layer, respectively; $\mu_{\max}$ and $\mu_{\min}$ are the maximum and minimum of Poisson's ratio of the calculated layers, respectively; and A_1 and A_2 are the weight coefficients of the two factors, which are generally taken as 0.5.

The fracture toughness index (K_{IC}) is calculated as follows [50]:

$$K_{IC} = 0.313 + 0.0027E. \tag{7}$$

4. Geomechanical Analysis Results

4.1. Geomechanical Histogram. In this study, the geomechanical evaluation of several wells in the Dibei gas reservoir is conducted, and the rock mechanical properties, in situ stress, and distribution characteristics of fractures in the wellbore are defined. Taking Well DX1 as an example (Figure 10), the elastic modulus in Well DX 1 mainly ranges between 18 GPa and 30 GPa, with a median of 23 GPa. Among them, the elastic modulus in J_1a^1 and J_1a^2 is slightly lower, with a median of 22 GPa, and that of J_1a^3 is slightly higher, with a median of 27 GPa. The elastic modulus of different lithologies is clearly different, approximately 24 GPa for sandstone and 27 GPa for mudstone. The uniaxial compressive strength mainly ranges between 80 MPa and 120 MPa, with a median of 110 MPa. The uniaxial compressive strength is slightly lower in the J_1a^1 and J_1a^2 sections, with a median of 98 MPa, and slightly higher in the J_1a^3 section, with a median of 111 MPa. From the perspective of lithology, the uniaxial compressive strength of sandstone is approximately 105 MPa and that of mudstone is 98 MPa. Poisson's ratio has little change in different layers of J_1a, at approximately 0.25. The in situ stress of Well DX1 is shown as $S_H > S_v > S_h$ and has obvious stratification. S_h is relatively high in the upper part of J_1a^1 and J_1a^2 (4710~4815 m), at 104 MPa, low in the lower part of J_1a^2 to the top of J_1a^3 (4815~4900 m), at 98 MPa, and high in the lower part of J_1a^3, at 105 MPa. The horizontal stress difference is approximately 35~40 MPa, and the local interval exceeds 40 MPa. The distribution trend in the wellbore is similar to S_h. The

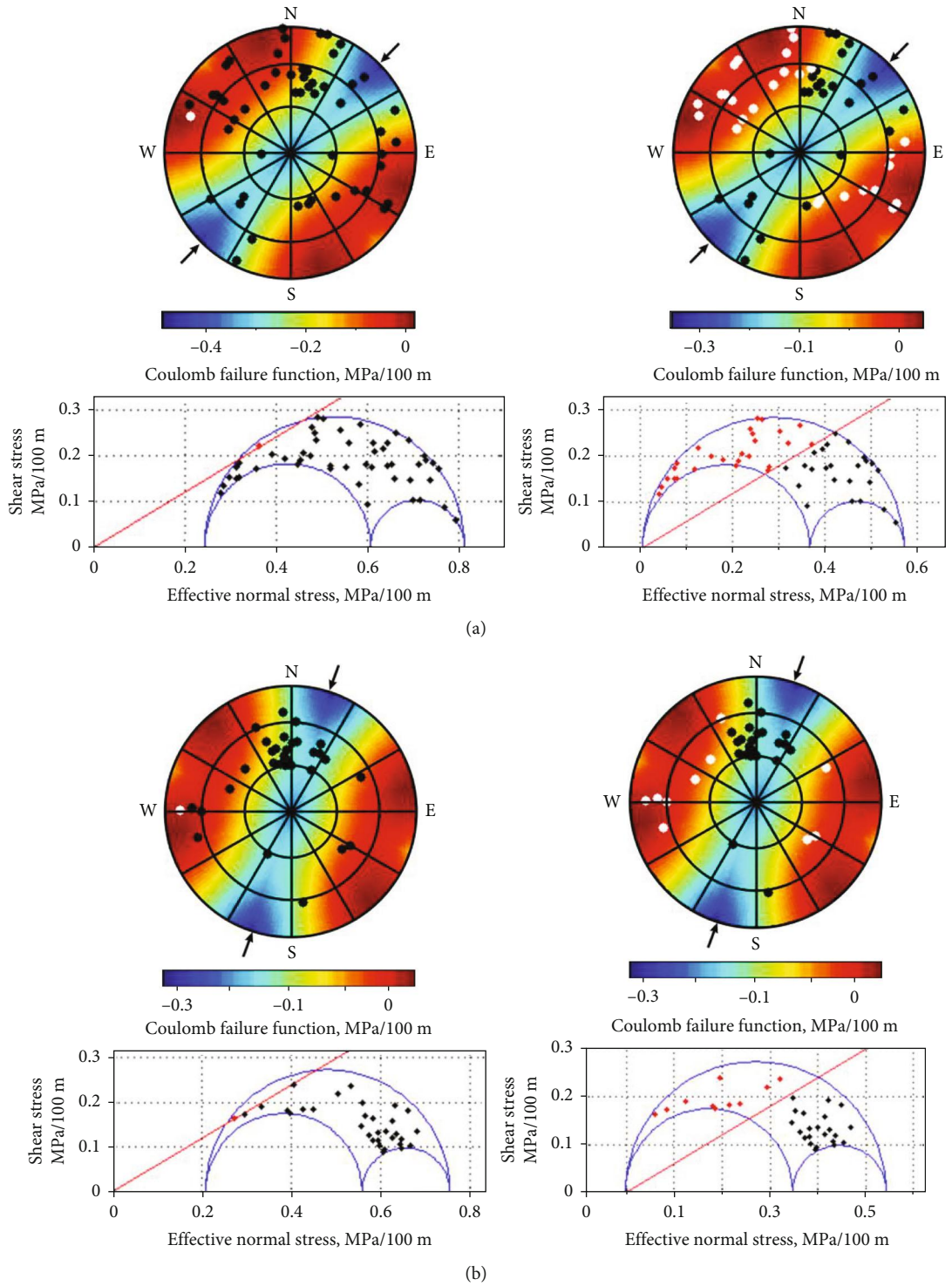

FIGURE 13: Fracture opening rate simulation results in the Dibei gas reservoir.

brittleness index of reservoir rocks is generally high. In locally thick mudstone intervals (4868~4885 m), the value is low. The fracturing index is generally 0.6, which is high in the interval with low in situ stress and well-developed fractures. Natural fractures of Well DX 1 are mainly developed in the lower part of J_1a^2 (4820~4870 m), and there are few fractures in the J_1a^3 section.

It can be seen from the gas production section in Well DX 1 (Figure 10) that not all intervals produce gas, and natural gas only comes from local favorable intervals. Within the range of 4819~4830 m, the gas production is 20×10^4 m^3, accounting for 88% of the total gas production of the well, and the gas production of other intervals is less than 12%. By analyzing the two main gas producing intervals, it

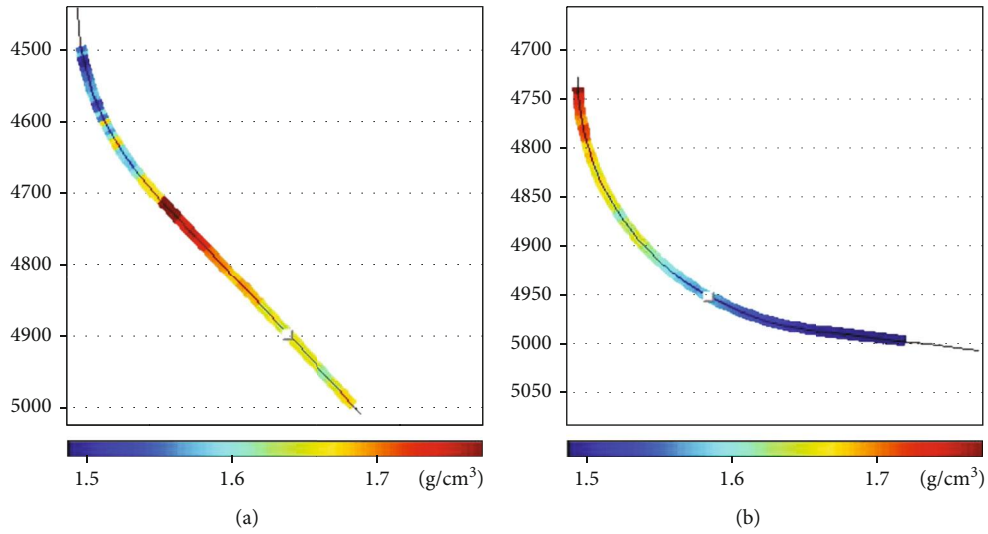

Figure 14: Simulation of the safe drilling fluid density window of the well trajectory with different well deviation angles.

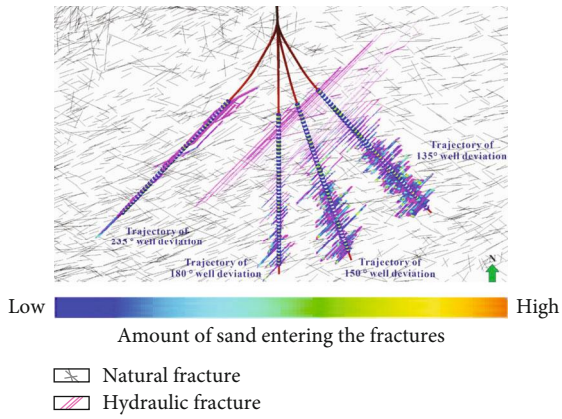

Figure 15: Hydraulic fracture network formed by fracturing in different drilling directions.

is found that they have the characteristics of low in situ stress, fracture development, and high fracturing index.

4.2. In Situ Stress. The in situ stress direction in the Dibei gas reservoir is determined by the breakout orientation (Figure 11). The results show that the S_H direction in the Dibei gas reservoir changes greatly and has poor regularity. The northern part of the gas reservoir is in the ~N–S direction. For those wells adjacent to the fault in the middle gas reservoir, the S_H direction deflects along the fault strike and shows a NE–SW direction.

In the study area, there are obvious differences in the in situ stress distribution among the wells of the Dibei gas reservoir. Compared with the Cretaceous reservoir of the Kelasu gas field in the Kuqa Depression, the Dibei gas reservoirs show poor in situ stress distribution regularity, and there is neither a "neutral surface effect" of the anticline structure nor a unified geomechanical sequence. For example, Well DX1 is 800 m away from Well DB105, and they have similar burial depths. However, the S_h in well DB105 is 20 MPa higher than that in well DX1, and there is no similarity in the longitudinal stratification characteristics of the in situ stress in the two wells. In addition, Well DB102 is more than 200 m deeper than most wells, such as Well YN2, but its S_h is 10 MPa lower, indicating that it has a low stress gradient (Figure 12).

4.3. Fracture Characteristics and Effectiveness Evaluation. Fractures in the Dibei gas reservoir are generally developed, and the overall strike is E–W-trending, but the fracture development characteristics among wells vary greatly, showing a strong heterogeneous distribution. For example, Well DX1 is a couple hundred meters away from Well YN 2; however, 29 fractures with different strikes are identified in Well DX1, and only two fractures with NNE–SSW strikes are identified in Well YN2. In addition, the fracture strike in Well DX1 and Well DB102 is discrete; it is mainly in the near east-west direction, followed by the northeast and northwest directions. The fracture tendency to the south and the overall fractures are distributed in a network, while fracture strike is basically the same in Well DB104, showing a group of nearly parallel shear fractures (Figure 11).

Based on the statistics of fracture angle, in the Dibei gas reservoir, most angles range between 45° and 75°, while the Kelasu gas field adjacent to the Dibei gas reservoir generally develops high-near vertical fractures (Figure 11).

Based on the critical stress fracture hypothesis, the opening rate of fractures in the Dibei gas reservoir under different injection pressures is evaluated. The opening simulation results of fractures in Well DX1 are shown in Figure 13(a). When the bottom net pressure is 1.86 MPa/100 m (88.4 MPa), one natural fracture opens with an opening rate of 2% (white points in stereogram and red point in Mohr's circle), and when it is 2.10 MPa/100 m (99.8 MPa), the opening rate is nearly 50%. Figure 13(b) shows the simulation

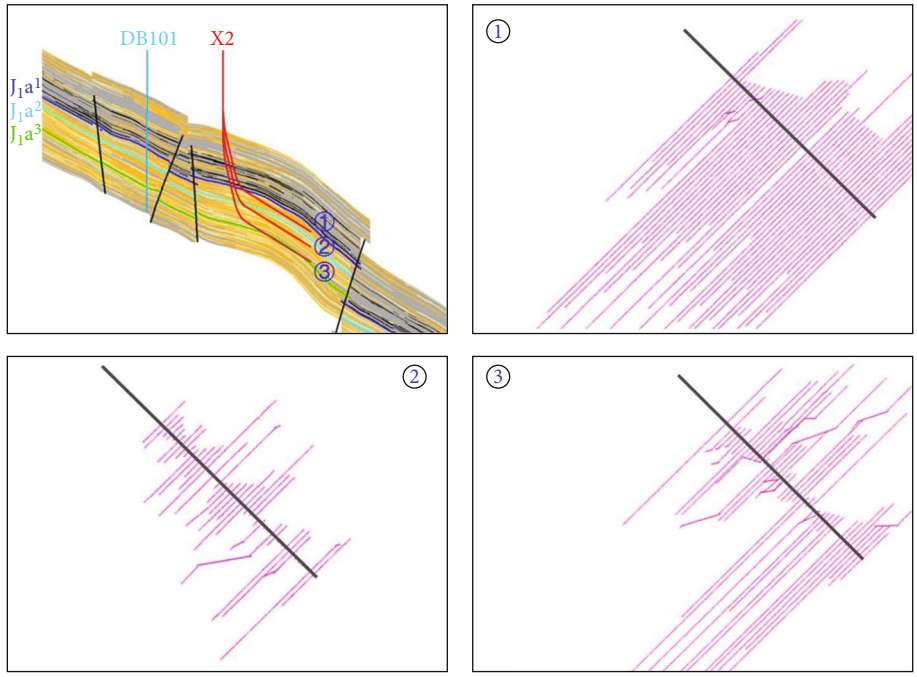

Figure 16: Simulation of the influence of different landing points on the fracture network.

results of fracture opening in Well DB102. When the bottom net pressure is 1.97 MPa/100 m (97.5 MPa), one fracture opens with an opening rate of 3%, and when it is 2.12 MPa/100 m (105.0 MPa), only 31% of the fractures are open. This shows that natural fractures of Well DX1 have a high opening rate during fracturing; however, it is low in Well DB104. As mentioned above, fractures with low opening pressure are prone to shear slip, have better permeability, and have better fracture effectiveness. Therefore, the fracture effectiveness is high in Well DX1 and low in Well DB102.

The daily natural gas output of Well DX1 is nearly $60 \times 10^4\ m^3$, and the oil output is more than $70\ m^3$. Well DB104 has a daily gas output of $70 \times 10^4\ m^3$. Both are high-yield wells in the Dibei gas reservoir. However, Well DB102 only obtains an output of after fracturing. This may indicate that fracture effectiveness has an obvious effect on oil and gas production.

5. Discussions

5.1. Geomechanical Factors for Increasing Production. Previous exploration and development practices in the Kuqa Depression show that the main gas producing intervals of deep tight fractured reservoirs generally have the characteristics of low in situ stress, fracture development, high fracture effectiveness, and a high fracturing ability index [29]. The difficulties encountered in previous explorations and developments can be explained from the perspective of geomechanics. For example, gas wells with similar petrophysical properties (including petrological characteristics, porosity, and permeability) in the same structure have large productivity differences, and even two adjacent wells in the same structure may be over 40 times the difference [29, 40]. The production of some wells with high porosity and permeability at the high place of an anticline structure is lower than that of wells with low porosity and permeability at the slightly lower part of the anticline. Therefore, deep oil and gas exploration methods cannot be limited to the traditional evaluation of reservoir quality, that is, based on the analysis of the porosity and permeability of reservoirs. It is necessary to strengthen the evaluation of rock mechanical behavior, fully consider the factors related to in situ stress, and find and efficiently develop deep high-quality reservoirs.

In addition, whether a deep oil and gas well can achieve high production depends not only on the reservoir quality but also on the success of fracturing. The fracturing of the Dibei gas reservoir has experienced a difficult process. In 1998, Well YN 2 was tested in the middle of the Ahe Formation and obtained a daily gas production of $10 \times 10^4\ m^3$. However, after acidizing and fracturing, the daily gas production is less than $5 \times 10^4\ m^3$, and after lateral drilling, the gas production is only $6 \times 10^4\ m^3$. In 2013, Well DiB101 was tested to have a daily gas production of $6 \times 10^4\ m^3$. After fracturing, the daily gas production is only more than $1000\ m^3$. In 2018, in Well DB105X, fracturing was conducted on the interval (4785~4849 m) with high physical properties, but the daily gas production was only about $8 \times 10^4\ m^3$. This shows that in the Dibei gas reservoir with complex geological conditions, only limited means of reservoir fracturing and stimulation are available, and the stimulation scheme lacks a scientific basis. Even if the formation is successfully fractured, high-yield oil and gas may not be obtained, and the open flow is difficult to be expected. The early fracturing of the Dibei gas reservoir

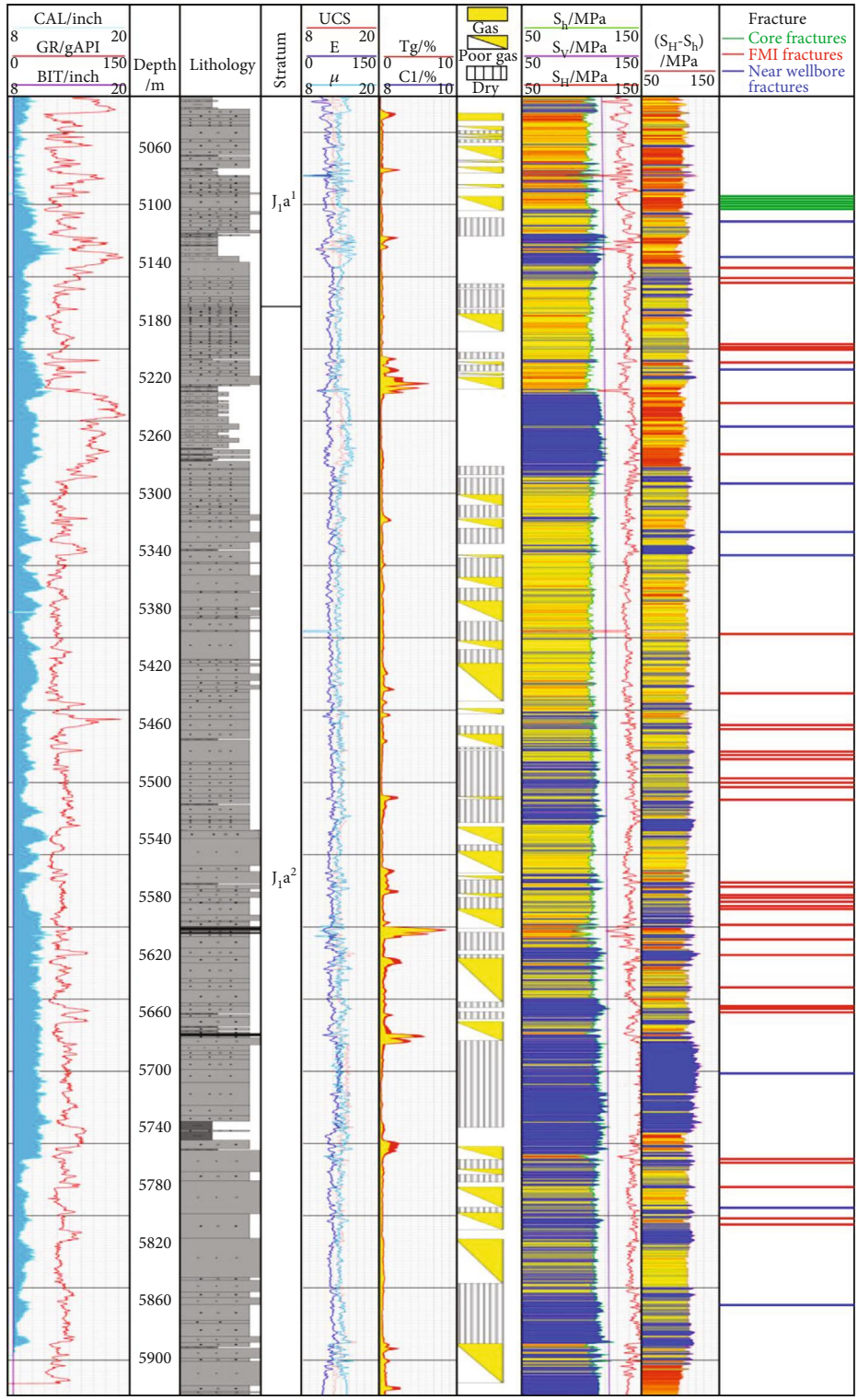

Figure 17: Geomechanical histogram of Well X2.

mainly focused on geological and engineering processes and relied on "great efforts to make miracles," causing a weak understanding of engineering geology and a lack of a set of well completion quality evaluation methods for deep reservoirs suitable for strong compression and poor stimulation effects.

5.2. Stimulation Technique considering Geomechanical Factors

5.2.1. Problems and Solutions of Location Deployment. One of the main problems in the exploration of the Dibei tight gas reservoir is the optimization of favorable areas and well

Table 1: Fracturing interval and transformation suggestions based on reservoir characteristics and geomechanical analysis.

Section	Depth (m)	Petrophysical characteristics	Geomechanical characteristics	Suggestions
I	5039.50-5099.50	The porosity of 4~8%, the permeability of $0.5\sim6\times10^{-3}$ μm^2, and the reservoir space consisting of intragranular solution pore, microfracture, and micropore	The minimum principal stress of 106 MPa on average and the fracture underdeveloped	It is suggested to carry out large-scale sand fracturing and fracture making to improve the permeability of the reservoir
II	5144.50-5223.00	The porosity of 4~8%, the permeability of $0.5\sim6\times10^{-3}$ μm2, and the reservoir space consisting of intragranular solution pore, microfracture, and micropore	10 high-angle fractures with minimum principal stress of 107 MPa	It is suggested to carry out sand fracturing to form fracture network and improve the permeability of the reservoir
III	5285.50-5321.50	The porosity of 4~8%, the permeability of $0.5\sim4\times10^{-3}$ μm^2, and the reservoir space consisting of intragranular solution pore, microfracture, and micropore	Two high-angle fractures with minimum principal stress of 109 MPa	It is suggested to carry out sand fracturing to form fracture network and improve the permeability of the reservoir
IV	5361.50-5387.80	Calcite cementation developed in the reservoir, the porosity of 4~6%, the permeability of $0.5\sim4\times10^{-3}$ μm^2, and the reservoir space consisting of intragranular solution pore, microfracture, and micropore	One high-angle fractures with minimum principal stress of 110 MPa	It is suggested to carry out sand fracturing to form fracture network and improve the permeability of the reservoir
V	5819.00-5839.00	Relatively tight reservoir, the porosity of 4~6%, the permeability of $0.5\sim4\times10^{-3}$ μm^2, and the reservoir space consisting of intragranular solution pore, microfracture, and micropore	One high-angle fracture with minimum principal stress of 110 MPa	It is suggested to carry out large-scale sand fracturing to form fracture network and improve the permeability of the reservoir

location deployment. Because the in situ stress and fracture effectiveness under its control have an obvious control on the productivity of the Dibei gas reservoir, the positions and intervals with low in situ stress, fracture development, and high fracture effectiveness are favorable parts. However, the distribution of in situ stress and natural fractures has great heterogeneity and anisotropy and is controlled by many factors, such as structural style, faults, fracture, lithology, and fluid. The in situ stress state, fracture development, and permeability of fractures in different directions vary greatly. Therefore, directional wells can overcome the problems of heterogeneity and anisotropy. We can adjust the borehole trajectory of directional wells according to the in situ stress and fracture distribution and drill toward favorable low-stress zones and fractures with high permeability. In addition, under the strike-slip stress regime in the Dibei gas reservoir, the borehole wall stability of inclined wells or horizontal wells is much better than that of vertical wells. The fracture development of the Dibei gas reservoir weakens the rock mass strength, increases the anisotropy, and reduces the borehole stability. However, if the directional borehole is perpendicular to the fracture surface, the shear stress acting on the fracture surface is zero, which can maintain high borehole wall stability. The above analysis shows that directional wells in the Dibei gas reservoir are more conducive to penetrating favorable areas than drilling vertical wells and ensuring drilling safety.

5.2.2. Problems and Solutions of Fracturing. In the process of fracturing, forming complex fractures is conducive to the communication between the reservoir and wellbore, but the fracture extension mode is greatly affected by in situ stress and natural fractures around the well [51–57]. It is necessary to predict the extension of fractures according to the magnitude and direction of in situ stress and the development of natural fractures around the well and select the interval with low difficulty and low risk of fracturing as the fracturing target interval. However, due to the great heterogeneity and anisotropy of the distribution of in situ stress and natural fractures, directional wells may solve the problem of fracturing as well. By simulating the extension of fractures in the borehole trajectory in different directions, the deviation azimuth and intervals can be determined and optimized for hydraulic fracturing to finally realize the stimulation of the tight gas reservoir.

In summary, a set of stimulation techniques considering geomechanical factors has been proposed, and its core is the quantitative optimization method of directional trajectory with "taking into account sweet spot penetration, borehole wall stability and conducive to fracturing," that is, considering the geomechanical factors for hydraulic fracturing from the source of borehole location deployment.

5.2.3. A Successful Case. Based on the above concept, Well X2, a highly deviated well, was deployed in the Dibei gas reservoir in 2020, which is a successful practice of stimulation techniques considering geomechanical factors.

First, based on 3D heterogeneous geomechanical modeling, the 3D rock mechanical parameters, 3D stress field, and fracture distribution characteristics of the Dibei gas reservoir are defined. Based on the structural characteristics, reservoir characteristics, and petroleum geological conditions, a favorable exploration area is selected. According to the surface conditions of avoiding high mountains, the well point is in

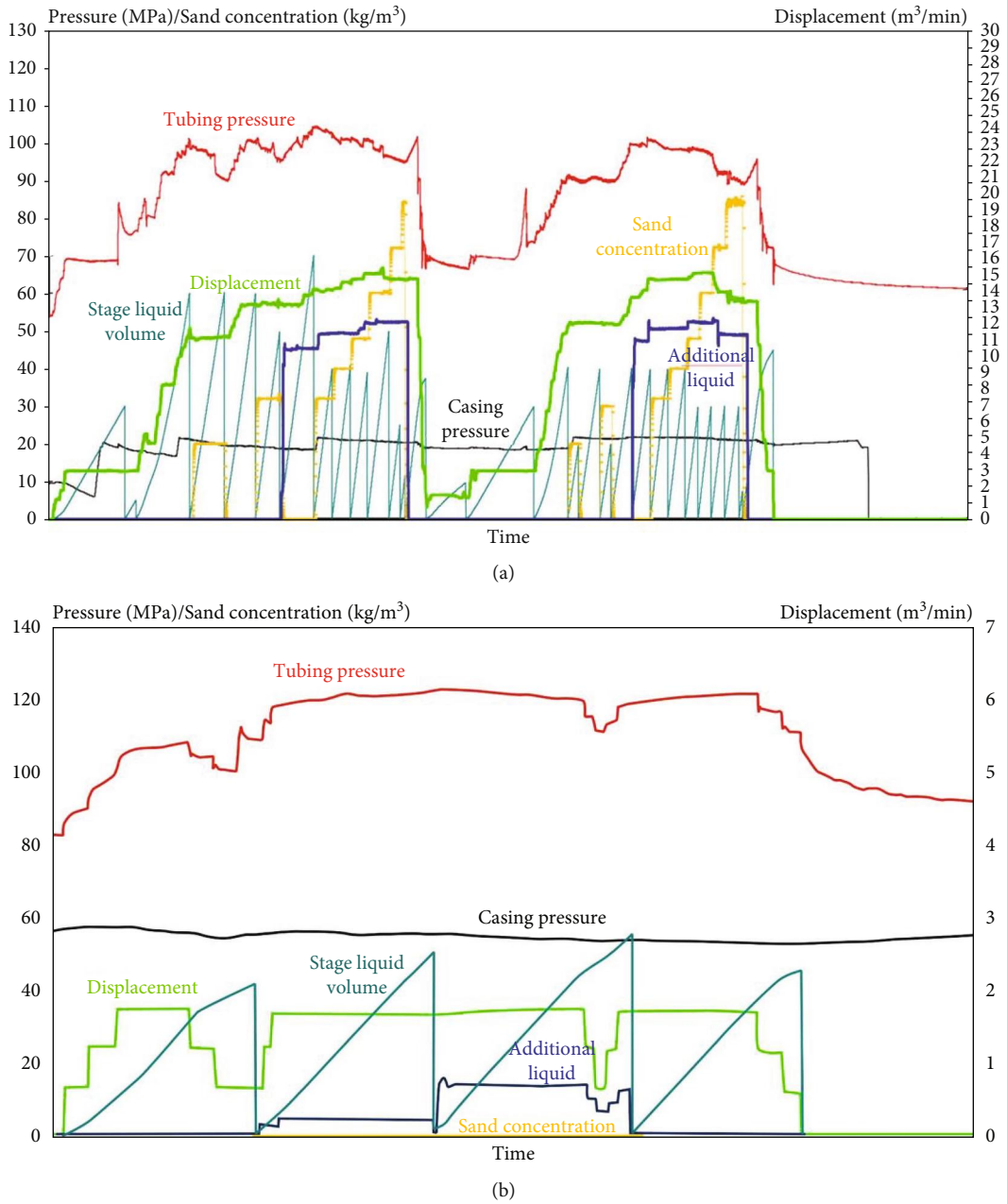

Figure 18: Comparison of fracturing operation curves. (a) Taking the fracturing operation curves of Section 4 as an example, it shows that under a displacement of 14 m^3/min and an oil pressure of 100~90 MPa, the fractures gradually expand and reach the equilibrium state. (b) Fracturing operation curve of a failed well in the Kuqa depression. In the case of a displacement of 1.5 m^3/min, the oil pressure may rise rapidly to the upper limit of 120 MPa and finally cause the failure of transformation due to difficult fracturing.

the north of the favorable area (Figure 2(a)). It is planned to drill in the south direction of the proposed exploration part by means of directional wells.

Second, the well type is further optimized according to the in situ stress and borehole wall stability. As shown in Figure 14, well trajectory safe drilling fluid density windows with different well deviation angles are simulated. The in situ stress field and the selected well location conditions result in a small well deviation angle (70°) and a wide borehole safe drilling fluid density window of about 0.42 g/cm^3. If a larger well deviation angle (nearly 90°) is used, the borehole safe drilling fluid density window will be narrow, at about 0.28 g/cm^3. Therefore, it is determined to adopt a highly deviated well with a deviation angle of approximately 70°.

Third, the deviation orientation is optimized according to the in situ stress, fracture and borehole wall stability. Considering that the fracture strike in the Dibei gas reservoir is mostly parallel to the fault strike, the dominant deviation orientation is NW–SW to ~N–S (135°~180°) to improve the probability of fracture penetration.

Fourth, the deviation orientation is optimized to facilitate fracturing. Fracture distribution simulation is conducted

for wells in different drilling directions. The same pumping procedure is adopted in each simulation, considering the anisotropy and heterogeneity of fracture permeability. Figure 15 shows the hydraulic fracture pattern formed by fracturing in different drilling directions. The S_H direction in the area is approximately 45°, and the main direction of the fracture is basically consistent with the S_H direction. In the case of a small angle between the borehole trajectory and the S_H direction, the hydraulic fracture is basically distributed along the borehole, and the coverage area of the fracture network is relatively small, such as the drilling direction of 235°. In the case of a large angle between the borehole trajectory and the S_H direction, the coverage area of the fracture network is large, such as the drilling direction of 135° and 150°. Based on this, the deviation orientation is determined to be 135°~150°.

Fifth, the impact of different landing points on the fracture network is simulated. As shown in Figure 16, the well deviation azimuth is set at 135°, and the well deviation angle is 70°. Scheme 1 forms the most compression fractures and extends the farthest, which is conducive to transformation and stimulation.

Geomechanical evaluation of Well X2 is carried out (Figure 17), and the in situ stress shows obvious segmentation with low stress in the upper parts of J_1a^1 and J_1a^2. Due to the poor imaging quality of FMI, the methods of drilling, leakage, core observation, remote detection, acoustic wave, and numerical simulation around the well are comprehensively used to determine the fracture development. The results show that Well X2 develops fractures to a certain extent.

Based on the analysis of reservoir petrophysical properties, combined with in situ stress, fracture, and other geomechanical parameters, five high-quality intervals are divided into fracturing intervals, and corresponding reconstruction suggestions are also proposed (Table 1). Figure 18(a) shows the fracturing operation curves of Section 4. Under a displacement of 14 m^3/min and an oil pressure of 100~90 MPa, the fractures gradually expand and reach the equilibrium state. Meanwhile, a connected fracture network has been formed in the reservoir. Figure 18(b) shows the fracturing operation curve of a failed well in the Kuqa depression. In the case of a displacement of 1.5 m^3/min, the oil pressure may rise rapidly to the upper limit of 120 MPa and finally cause the failure of transformation due to difficult fracturing.

6. Conclusions

(1) In the Dibei gas reservoir, the in situ stress and fracture distribution are highly heterogeneous, making reservoir quality evaluation and fracturing difficult. The suggestion of directional well drilling is put forward with stimulation technology considering geomechanical factors. The geomechanical factors should be fully considered in the location and trajectory optimization stage

(2) The stimulation of a deep tight sandstone gas reservoir lies in both reservoir quality and engineering factors. The geomechanical research defines the rock mechanical properties of the reservoir, in situ stress, and fracture characteristics and supports the quantitative optimization of the directional trajectory. The sweet spot penetration and borehole stability are considered, and the difficulty of fracturing is reduced, thereby facilitating the efficient stimulation of the tight gas reservoir

(3) Geomechanical research has strengthened the evaluation of rock mechanical behavior, built an integrated bridge between geology and engineering, replaced the working mode of separation of traditional geological research and engineering construction, and played an important role in the stimulation of unconventional resources such as ultradeep oil and gas, tight oil and gas, shale oil and gas, and coalbed methane

Data Availability

The data used to support the findings of this study are available from the corresponding author upon request.

Conflicts of Interest

The authors declare that they have no conflicts of interest.

Acknowledgments

This study is funded by the Major National Science and Technology Project (2016ZX05051) and the Major Science and Technology Project of PetroChina Company Limited (2018E-1803).

References

[1] K. E. Higgs, H. Zwingmaan, A. G. Reyes, and R. H. Funnnell, "Diagenesis, porosity evolution, and petroleum emplacement in tight gas reservoirs, Taranaki Basin, New Zealand," *Journal of Sedimentary Research.*, vol. 77, no. 12, pp. 1003–1025, 2007.

[2] X. Q. Pang, X. H. Shao, M. W. Li et al., "Correlation and difference between conventional and unconventional reservoirs and their unified genetic classification," *Gondwana Research*, vol. 97, no. 6, pp. 73–100, 2021.

[3] C. N. Zou, Z. Yang, G. S. Zhang et al., "Establishment and practice of unconventional oil and gas geology," *Acta Geologica Sinica*, vol. 93, no. 1, pp. 12–23, 2019.

[4] G. X. Li, Z. D. Lei, W. H. Dong, H. Y. Wang, X. F. Zheng, and J. Tan, "Progress, challenges and prospects of unconventional oil and gas development of CNPC," *China Petroleum Exploration*, vol. 27, no. 1, pp. 1–11, 2022.

[5] B. S. Aadnoy, "Geomechanics in the oil industry-what have we learned and where do we go?," in *Proceedings of the Sixth World Congress on Computational Mechanics in Conjunction with the Second Asian-Pacific Congress on Computational Mechanics*, pp. 168–170, Beijing, 2004.

[6] M. A. Addis, "The geology of geomechanics: petroleum geomechanical engineering in field development planning," *Geological Society, London, Special Publications*, vol. 458, no. 1, pp. 7–29, 2017.

[7] S. X. Sang, X. Z. Zhou, S. Q. Liu et al., "A review of mechanical stratigraphy methodology and its application in high-efficient exploration and development of coal measure gas," *Acta Geologica Sinica*, vol. 96, no. 1, pp. 304–316, 2022.

[8] A. Sangnimnuan, J. Li, and K. Wu, "Development of efficiently coupled fluid-flow/geomechanics model to predict stress evolution in unconventional reservoirs with complex-fracture geometry," *SPE Journal*, vol. 23, no. 3, pp. 640–660, 2018.

[9] X. Y. Guo, H. Q. Song, K. Wu, and J. Killough, "Pressure characteristics and performance of multi-stage fractured horizontal well in shale gas reservoirs with coupled flow and geomechanics," *Journal of Petroleum Science and Engineering*, vol. 163, pp. 1–15, 2018.

[10] W. Ju, Z. L. Li, W. F. Sun, and H. R. Xu, "In-situ stress orientations in the Xiagou tight oil reservoir of Qingxi Oilfield, Jiuxi Basin, northwestern China," *Marine and Petroleum Geology*, vol. 98, pp. 258–269, 2018.

[11] A. Kingdon, M. W. Fellgett, and J. D. O. Williams, "Use of borehole imaging to improve understanding of the in-situ stress orientation of Central and Northern England and its implications for unconventional hydrocarbon resources," *Marine and Petroleum Geology*, vol. 73, pp. 1–20, 2016.

[12] J. S. Liu, G. J. Zhang, J. P. Bai, W. L. Ding, H. M. Yang, and Y. Liu, "Quantitative prediction of the drilling azimuth of horizontal wells in fractured tight sandstone based on reservoir geomechanics in the Ordos Basin, central China," *Marine and Petroleum Geology*, vol. 136, article 105439, 2022.

[13] M. Rajabi, M. Tingay, and O. Heidbach, "The present-day state of tectonic stress in the Darling Basin, Australia: implications for exploration and production," *Marine and Petroleum Geology*, vol. 77, pp. 776–790, 2016.

[14] A. Rezaei, F. Siddiqui, B. Dindoruk, and M. Y. Soliman, "A review on factors influencing the rock mechanics of the gas bearing formations," *Journal of Natural Gas Science and Engineering*, vol. 80, article 103348, 2020.

[15] M. Tingay, R. R. Hillis, C. K. Morley, R. C. King, R. E. Swarbrick, and A. R. Damit, "Present-day stress and neotectonics of Brunei: implications for petroleum exploration and production," *AAPG Bulletin*, vol. 93, no. 1, pp. 75–100, 2009.

[16] P. W. Zhang, X. Liang, C. G. Xian, B. G. Liu, W. X. Wang, and C. Zhang, "Geomechanics simulation of stress regime change in hydraulic fracturing: a case study," *Geomechanics and Geophysics for Geo-Energy and Geo-Resources*, vol. 8, no. 2, pp. 1–18, 2022.

[17] Z. Wang, "Formation mechanism and enrichment regularities of Kelasu subsalt deep large gas field in Kuqa Depression, Tarim Basin," *Natural Gas Geoscience*, vol. 25, no. 2, pp. 153–166, 2014.

[18] Y. G. Tang, X. Z. Yang, H. W. Xie, Z. P. Xu, H. X. Wei, and Y. N. Xie, "Tight gas reservoir characteristics and exploration potential of Jurassic Ahe Formation in Kuqa Depression, Tarim Basin," *China Petroleum Exploration*, vol. 26, no. 4, pp. 113–124, 2021.

[19] W. Ju, G. T. Hou, S. Y. Huang, and K. X. Ren, "Structural fracture distribution and prediction of the Lower Jurassic Ahe Formation sandstone in the Yinan-Tuzi area, Kuqa Depression," *Geotectonica et Metallogenia*, vol. 37, no. 4, pp. 592–602, 2013.

[20] K. Wang, A. C. Xiao, T. Cao, R. H. Zhang, H. X. Wei, and C. F. Yu, "Geological structures and petroleum exploration fields of the northern tectonic belt in the Kuqa depression, Tarim basin," *Acta Geologica Sinica*, vol. 96, no. 2, pp. 368–386, 2022.

[21] N. T. T. Binh, T. Tokunaga, H. P. Son, and M. V. Binh, "Present-day stress and pore pressure fields in the Cuu Long and Nam Con Son basins, offshore Vietnam," *Marine and Petroleum Geology*, vol. 24, no. 10, pp. 607–615, 2007.

[22] S. Brooke-Barnett, T. Flottmann, P. K. Paul et al., "Influence of basement structures on in situ stresses over the Surat Basin, Southeast Queensland," *Journal of Geophysical Research: Solid Earth*, vol. 120, no. 7, pp. 4946–4965, 2015.

[23] W. Ju, J. Shen, Y. Qin et al., "In-situ stress state in the Linxing region, eastern Ordos Basin, China: implications for unconventional gas exploration and production," *Marine and Petroleum Geology*, vol. 86, pp. 66–78, 2017.

[24] T. Engelder, *Stress Regimes in the Lithosphere*, Princeton University Press, Princeton, 1993.

[25] J. S. Bell, "In-situ stress and coal bed methane potential in Western Canada," *Bulletin of Canadian Petroleum Geology*, vol. 54, no. 3, pp. 197–220, 2006.

[26] M. Tingay, R. R. Hills, C. K. Morley, R. Swarbrick, and E. Okpere, "Variation in vertical stress in the Baram Basin, Brunei: tectonic and geomechanical implications," *Marine and Petroleum Geology*, vol. 20, no. 10, pp. 1201–1212, 2003.

[27] M. D. Zoback, C. A. Barton, M. Brudy et al., "Determination of stress orientation and magnitude in deep wells," *International Journal of Rock Mechanics and Mining Sciences*, vol. 40, no. 7-8, pp. 1049–1076, 2003.

[28] Z. M. Li and J. Z. Zhang, *In-Situ Stress and Exploration and Development of Oil and Gas*, Petroleum Industry Press, Beijing, 1997.

[29] K. Xu, H. Zhang, R. Dong et al., "In situ stress distribution in cretaceous ultra-deep gas field from 1D mechanical earth model and 3D heterogeneous geomechanical model, Kuqa Depression, Tarim Basin, NW China," *Frontiers in Earth Science*, vol. 10, article 937393, 2022.

[30] M. D. Zoback, *Reservoir Geomechanics*, Cambridge University Press, Cambridge, 2007.

[31] L. Gong, J. Wang, S. Gao et al., "Characterization, controlling factors and evolution of fracture effectiveness in shale oil reservoirs," *Journal of Petroleum Science and Engineering*, vol. 203, no. 2, article 108655, 2021.

[32] W. Ju, X. B. Niu, S. Y. Feng, Y. You, H. R. Xu, and S. Y. Wang, "The present-day in-situ stress state and fracture effectiveness evaluation in shale oil reservoir: a case study of the Yanchang formation Chang 7 oil-bearing layer in the Ordos Basin," *Journal of China University of Mining & Technology*, vol. 49, no. 5, pp. 931–940, 2020.

[33] S. Y. Li, X. M. Tang, J. He, S. Xu, F. T. Sun, and Y. D. Su, "Fracture characterization combining acoustic reflection imaging and rock mechanics," *Acta Petrolei Sinica*, vol. 41, no. 11, pp. 1388–1395, 2020.

[34] Y. L. Lu, H. Z. Lyu, Y. J. Cui, and H. B. Chen, "Method for fracture effectiveness evaluation based on 3D Mohr Circle and its application," *Acta Petrolei Sinica*, vol. 39, no. 5, pp. 564–569, 2018.

[35] Z. Mao, L. B. Zeng, G. P. Liu et al., "Characterization and effectiveness of natural fractures in deep tight sandstones at the south margin of the Junggar Basin, northwestern China," *Oil & Gas Geology*, vol. 41, no. 6, pp. 1212–1221, 2020.

[36] J. X. Shi, L. B. Zeng, Q. S. Tan, J. P. Wang, Y. Z. Li, and H. W. Li, "Effectiveness of natural fractures in CBM reservoirs and its influence on CBM development in the southern Qinshui Basin," *Oil & Gas Geology*, vol. 41, no. 3, pp. 617–626, 2020.

[37] J. S. Liu, H. M. Yang, K. Xu et al., "Genetic mechanism of transfer zones in rift basins: insights from geomechanical models," *GSA Bulletin.*, vol. 134, no. 9-10, pp. 2436–2452, 2022.

[38] K. Xu, H. Zhang, H. Y. Wang et al., "3D geomechanical modeling and prediction of fractures in the Bozi ultra-deep gas field in the Kuqa Depression of Tarim Basin," *Frontiers in Earth Science*, vol. 10, article 863033, 2022.

[39] K. Xu, H. Yang, Z. Hui et al., "Fracture effectiveness evaluation in ultra-deep reservoirs based on geomechanical method, Kuqa Depression, Tarim Basin, NW China," *Journal of Petroleum Science and Engineering*, vol. 215, article 110604, 2022.

[40] T. W. Jiang, H. Zhang, K. Xu et al., "Technology and practice for quantitative optimization of borehole trajectory in ultra-deep fractured reservoir: a case study of Bozi A gas reservoir in Kelasu structural belt, Tarim Basin," *China Petroleum Exploration*, vol. 26, no. 4, pp. 149–161, 2021.

[41] C. A. Barton, M. D. Zoback, and D. Moos, "Fluid flow along potentially active faults in crystalline rock," *Geology*, vol. 23, no. 8, pp. 683–686, 1995.

[42] M. D. Zoback and P. Peska, "In-situ stress and rock strength in the GBRN/DOE pathfinder well, South Eugene Island, Gulf of Mexico," *Journal of Petroleum Technology*, vol. 47, no. 7, pp. 582–585, 1995.

[43] J. Byerlee, V. Mjachkin, R. Summers, and O. Voevoda, "Structures developed in fault gouge during stable sliding and stick-slip," *Tectonophysics*, vol. 44, no. 1-4, pp. 161–171, 1978.

[44] H. Y. Diao, "Rock mechanical properties and brittleness evaluation of shale reservoir," *Acta Petrologica Sinica*, vol. 29, no. 9, pp. 3300–3306, 2013.

[45] D. M. Jarvie, R. J. Hill, T. E. Ruble, and R. M. Pollastro, "Unconventional shale-gas systems: the Mississippian Barnett shale of north-central Texas as one model for thermogenic shale-gas assessment," *AAPG Bulletin*, vol. 91, no. 4, pp. 475–499, 2007.

[46] K. R. Qian, T. Liu, J. Z. Liu, X. W. Liu, Z. L. He, and D. L. Jiang, "Construction of a novel brittleness index equation and analysis of anisotropic brittleness characteristics for unconventional shale formations," *Petroleum Science*, vol. 17, no. 1, pp. 70–85, 2020.

[47] R. Rickman, M. J. Mullen, J. E. Petre, W. V. Grieser, and D. Kundert, "A practical use of shale petrophysics for stimulation design optimization: all shale plays are not clones of the Barnett shale," in *SPE Annual Technical Conference and Exhibition, SPE-115258-MS*, Denver, Colorado, USA, 2008.

[48] X. C. Jin, S. N. Shah, J. C. Roegiers, and B. Zhang, "Fracability evaluation in shale reservoirs-an integrated petrophysics and geomechanics approach," in *SPE Hydraulic Fracturing Technology Conference, SPE-168589-MS*, The Woodlands, Texas, USA, 2014.

[49] H. Li, "Research progress on evaluation methods and factors influencing shale brittleness: a review," *Energy Reports*, vol. 8, pp. 4344–4358, 2022.

[50] H. Zhang, G. Q. Yin, Z. M. Wang, and H. Y. Wang, "Fracability evaluation of deep-burial fractured sandstone gas reservoir in Kuqa depression," *Xinjiang Petroleum Geology*, vol. 40, no. 1, pp. 108–115, 2019.

[51] P. Tan, H. Pang, R. Zhang et al., "Experimental investigation into hydraulic fracture geometry and proppant migration characteristics for southeastern Sichuan deep shale reservoirs," *Journal of Petroleum Science and Engineering*, vol. 184, article 106517, 2020.

[52] L. Huang, J. Liu, F. Zhang, H. Fu, H. Zhu, and B. Damjanac, "3D lattice modeling of hydraulic fracture initiation and near-wellbore propagation for different perforation models," *Journal of Petroleum Science and Engineering*, vol. 191, article 107169, 2020.

[53] N. K. Potluri, D. Zhu, and A. D. Hill, "The effect of natural fractures on hydraulic fracture propagation," in *SPE European Formation Damage Conference, SPE-94568-MS*, Sheveningen, The Netherlands, 2005.

[54] J. Tian, H. Y. Liu, X. Q. Teng, Z. Z. Cai, H. Zhang, and L. H. Cao, "Geology-engineering integration practices throughout well lifecycle in ultra-deep complex gas reservoirs of Kelasu tectonic belt, Tarim Basin," *China Petroleum Exploration*, vol. 24, no. 2, pp. 165–173, 2019.

[55] T. Wang, W. R. Hu, D. Elsworth, W. Zhou, X. Y. Zhao, and L. Z. Zhao, "The effect of natural fractures on hydraulic fracturing propagation in coal seams," *Journal of Petroleum Science and Engineering*, vol. 150, pp. 180–190, 2017.

[56] K. Xu, J. Tian, H. J. Yang et al., "Prediction of current in-situ stress filed and its application of deeply buried tight reservoir, a case study of Keshen 10 gas reservoir in Kelasu structural belt, Tarim Basin," *Journal of China University of Mining & Technology*, vol. 49, no. 4, pp. 708–720, 2020.

[57] J. S. Liu, L. F. Mei, W. L. Ding, K. Xu, H. M. Yang, and Y. Liu, "Asymmetric propagation mechanism of hydraulic fracture networks in continental reservoirs," *GSA Bulletin.*, 2022.